

SPECTRAL PROPERTIES OF BLAST WAVE MODELS OF GAMMA-RAY BURST SOURCES

P. Mészáros¹, M.J. Rees² and H. Papathanassiou¹

¹ Pennsylvania State University, 525 Davey Lab., University Park, PA 16802

² Institute of Astronomy, Madingley Road, Cambridge CB3 0HA, England

Ap.J., Received: 11/19/93; Accepted:

Abstract

We calculate the spectrum of blast wave models of gamma-ray burst sources, for various assumptions about the magnetic field density and the relativistic particle acceleration efficiency. For a range of physically plausible models we find that the radiation efficiency is high, and leads to nonthermal spectra with breaks at various energies comparable to those observed in the gamma-ray range. Radiation is also predicted at other wavebands, in particular at X-ray, optical/UV and GeV/TeV energies. We discuss the spectra as a function of duration for three basic types of models, and for cosmological, halo and galactic disk distances. We also evaluate the gamma-ray fluences and the spectral characteristics for a range of external densities. Impulsive burst models at cosmological distances can satisfy the conventional X-ray paucity constraint $S_x/S_\gamma \lesssim$ few percent over a wide range of durations, but galactic models can do so only for bursts shorter than a few seconds, unless additional assumptions are made. The emissivity is generally larger for bursts in a denser external environment, with the efficiency increasing up to the point where all the energy input is radiated away.

1. Introduction

In most gamma-ray burst (GRB) scenarios, the very high initial radiation density leads to a relativistically expanding fireball. This is unavoidable if the GRB occur at cosmological distances (Paczynski, 1986, Goodman, 1986), and is also expected in many galactic models. For pair-dominated fireballs, an energetic but very short burst is obtained, whereas in the more common baryon-dominated fireballs most of the initial thermal energy gets converted into kinetic energy before it can be radiated away (Cavallo and Rees, 1978, Paczynski, 1990, Shemi and Piran, 1991), and only a weak burst is expected. However the kinetic energy of the coasting baryons can be reconverted into radiation when the ejecta are decelerated by the external medium (Rees and Mészáros, 1992, Mészáros and Rees, 1993).

This solves the total energy problem; it also results in an observable burst with a longer timescale since this is then determined by the dynamic timescale at the deceleration radius. For magnetically dominated fireballs the relativistic outflow is predominantly in the form of Poynting flux (e.g. Narayan, Paczyński and Piran, 1992, Usov, 1992). In all cases, a blast wave moves ahead of the contact discontinuity, while a reverse compression shock moves into the ejecta, randomizing the directed kinetic energy of the fireball. These shocks can accelerate particles which, in the presence of magnetic fields (either frozen-in or created by turbulent instabilities) lead to a radiation burst whose total energy is comparable to the initial energy input and whose time-delayed duration in the observer frame is comparable to that observed.

The radiation in these models depends on the efficiency of particle acceleration behind the shocks and on the magnetic field strength. The details of the particle acceleration process in relativistic shocks are uncertain, as are the mechanisms determining the magnetic energy density. We therefore explore various possibilities. Our first aim is to discover what range of parameters (e.g. expansion bulk Lorentz factors, external density) result in gamma-ray production with an efficiency and timescale appropriate for the observed bursts. Secondly, we consider the spectrum of the resulting radiation, and particularly the extension of this spectrum towards both softer and harder energies. This is interesting, among other reasons, because of the well-known ‘X-ray paucity constraint’ on some observed bursts. In our models, the spectra generally consist of two or more components, and are therefore not a simple power-law. The relative intensities in the different bands depend on the frequencies at which the breaks between these components occur. Observations (or even upper limits) in the X-ray band, or in the optical and UV, can therefore help to pin down the parameters of the model.

Our relativistic blast wave models were originally applied to cosmological bursts. However, the same phenomenon would occur, on a smaller scale, when relativistic plasma released, e.g., by magnetospheric disturbances on a galactic neutron star runs into the interstellar medium (Begelman, Mészáros and Rees, 1993). Our considerations are therefore also relevant for galactic models of gamma-ray burst sources, if one assumes that sufficient sources with the appropriate energy are available. We stress, however, that the blast wave burst model is insensitive to the specific energy input source. It is almost irrelevant whether the initial energy source is a merging neutron star binary, a failed supernova, a collapse-induced giant magnetic flare, or any other process with the right total energy. In this paper we examine the efficiency, duration and spectral properties of both galactic and extragalactic GRB blast wave models.

2. The Shock Burst Scenario

2.1 Standard Parameters and Basic Picture

For a fireball moving into an external medium characteristic of a cosmological scenario, the typical parameters are $n_{ext} \sim 1 n_0 \text{ cm}^{-3}$, $E_o \sim 10^{51} E_{51} \text{ ergs}$, $\eta \sim 10^3 \eta_3$, where E_o is the initial fireball energy, $\eta = E_o/M_o c^2$, M_o is the entrained baryon mass and n_{ext}

is the density of the external medium into which the fireball expands. The input total energy E_o may be initially dominated by either a radiation/pair mixture or by magnetic fields, depending on the initial conditions of the burst. The corresponding numbers for a galactic scenario would be $n_{ext} \sim 10^{-3} n_{-3} \text{ cm}^{-3}$, $E_o \sim 10^{41} E_{41} \text{ ergs}$, $\eta \sim 10^2 \eta_2$ (halo) and $n_{ext} \sim 1 n_0 \text{ cm}^{-3}$, $E_o = 10^{39} E_{39} \text{ ergs}$, $\eta = 10^2 \eta_2$ (disk). The bulk Lorentz factor initially grows as $\Gamma(r) \propto r$, and eventually saturates to the value $\Gamma_f \sim \eta$, when the internal energy per baryon becomes non-relativistic. Acceptable models for impulsive fireballs generally require $\eta \lesssim 10^3 - 10^4$ (e.g. Mészáros and Rees, 1993) in order for the burst energy and timescale not to be too low. The observer-frame deceleration radius r_d , and the corresponding comoving-frame expansion timescale t_{ex} and density of the ejecta material, are, for these three scenarios,

$$r_d \sim 10^{16} n_0^{-1/3} E_{51}^{1/3} \theta^{-2/3} \eta_3^{-2/3} \text{ cm} \sim 2.2 \times 10^{14} n_{-3}^{-1/3} E_{41}^{1/3} \theta^{-2/3} \eta_2^{-2/3} \text{ cm} \sim 4.6 \times 10^{12} n_0^{-1/3} E_{39}^{1/3} \theta^{-2/3} \eta_2^{-2/3} \text{ cm} \quad (2.1.1)$$

$$t_{ex} \sim 10^3 n_0^{-1/3} E_{51}^{1/3} \theta^{-2/3} \eta_3^{-5/3} \text{ s} \sim 2.2 \times 10^2 n_{-3}^{-1/3} E_{41}^{1/3} \theta^{-2/3} \eta_2^{-5/3} \text{ s} \sim 4.6 n_0^{-1/3} E_{39}^{1/3} \theta^{-2/3} \eta_2^{-5/3} \text{ s} , \quad (2.1.2)$$

$$n_d \sim 10^6 n_0 \eta_3^2 \text{ cm}^{-3} \sim 10^2 n_0 \eta_2^2 \text{ cm}^{-3} \sim 10^{-1} n_{-3} \eta_2^2 \text{ cm}^{-3} , \quad (2.1.3)$$

where η is the bulk Lorentz factor at the start of deceleration and θ is the opening half-angle (if not spherical) along which the fireball expands. The observed (lab frame) burst duration is η times shorter than the comoving dynamic time t_{ex} , i.e.,

$$t_L \sim 1 n_0^{-1/3} E_{51}^{1/3} \theta^{-2/3} \eta_3^{-8/3} \text{ s} \sim 2.2 n_{-3}^{-1/3} E_{41}^{1/3} \theta^{-2/3} \eta_2^{-8/3} \text{ s} \sim 4.6 \times 10^{-2} n_0^{-1/3} E_{39}^{1/3} \theta^{-2/3} \eta_2^{-8/3} \text{ s} . \quad (2.1.4)$$

Generally the deceleration of the ejecta occurs after the bulk Lorentz factor has saturated, $r_d \gg r_s \sim \eta r_o$, and also after $r_d \gg r_b \sim \eta^2 r_o$ (Mészáros, Laguna and Rees, 1993), so the lab-frame expansion time $t_L \sim r_d c^{-1} \eta^{-2} \gg r_o/c \sim 10^{-4} r_6 \text{ s}$ is of the order of seconds, and occurs well after the pairs of the ejecta drop out of equilibrium. (The ejecta become optically thin to baryonic electrons at a radius smaller than the deceleration radius, when a weak and very brief burst of $t_t \sim r_o/c \sim 10^{-4} \text{ s}$ is produced which precedes the shock burst by a time of order $\sim t_L$).

A strong relativistic blast wave moves ahead of the fireball. This blast wave decelerates as it sweeps up external matter; a reverse shock wave starts to move into the ejecta, and becomes marginally relativistic when the expanding ejecta reach a radius $\sim r_d$. New pairs may be formed in these shocks, whose maximum effect on the opacity can be evaluated by estimating the comoving compactness parameter at the deceleration radius, assuming all the kinetic energy available is converted into radiation above the pair formation threshold. This is $\tau_{\pm} \sim L \sigma_T / m_e c^3 \Delta R \sim n_{\pm} \sigma_T \Delta R \sim 10^{-3} E_{51}^{1/3} n_0^{2/3} \theta^{4/3} \eta_3^{1/3} \sim 10^{-8} E_{41}^{1/3} n_{-3}^{2/3} \theta^{4/3} \eta_2^{1/3} \ll 1$, i.e. both shocks are optically thin to pair formation (and also

to baryonic electrons). The spectrum of the radiation produced by the shocks is therefore virtually assured to be *non-thermal*, since the shocked electrons are relativistic and emit in an optically thin environment. Indeed, anything other than a non-thermal spectrum would be surprising under these circumstances.

The foregoing discussion, which treats the primary energy production as instantaneous, is self-consistent provided that the fireball is created in a time short compared with t_L . The actual energy release will, of course, really have a finite duration, and the fireball's early development will depend on the time-history of the energy production and on the behavior of η . An interesting possibility, especially relevant to 'cosmological' models which invoke a coalescing compact binary, is that the primary energy emerges as a magnetically-dominated wind lasting for up to a few seconds (e.g. Narayan *et al.* 1992; Usov 1992,1993). Some gamma rays may come directly from the inner part of the wind (just as they can come from the 'thinning' stage of an impulsive fireball). However, just as in the impulsive case, the wind will inflate a cavity, piling up external matter behind a blast wave, and may thereby convert its energy into gamma rays more efficiently.

To explore fully the consequences of non-impulsive (and possibly time-dependent) energy release, one would need to introduce further parameters. It is premature to do this in an elaborate way. It is, however, worthwhile and interesting to consider a simple (and physically plausible) illustrative case when the wind itself is unloaded and almost purely electromagnetic, so that its speed is not significantly below c . Suppose this wind turns on at $t = 0$, and maintains a steady isotropic energy flux L for a time t_w . It will inflate a spherical cavity of radius r . If the contact discontinuity at the cavity boundary expands with a Lorentz factor $\Gamma(r)$, the wind pressure, in the frame of the contact discontinuity, is proportional to $L/r^2\Gamma^2$. This would be balanced by the pressure of the shocked material between the blast wave and the shock discontinuity, which scales as $n_{ext}\Gamma^2$. The expansion Lorentz factor will be that for which these two forces balance, and this implies $\Gamma \propto r^{-1/2}n_{ext}^{-1/4}$.

When the wind ceases, at a time t_w after it switches on (measured in the observer frame), the part of the blast wave directed towards the observer will have reached a radius $r = \Gamma^2 ct_w$ and η will have fallen (owing to the 'loading' by swept-up matter) to $\sim (L/4\pi c^2 t_w^2 n_{ext})^{1/8}$. At that stage, the configuration would be essentially equivalent to a fireball where $E = Lt_w$ and where η has the value defined above. For these values, we find (as consistency requires) that the value of t_L given by (2.1.4) is indeed equal to t_w .

Although we present our subsequent discussion in terms of impulsively-produced pair, baryon or magnetically dominated fireballs, from the above discussion it applies equally to the corresponding wind models at the phase $t \simeq t_L$ when they are releasing most of their energy. The radiation from an impulsively-produced homogeneous fireball rises to a peak after a time $\sim r_d c^{-1} \eta^{-2}$ and then fades. The details of the initial rise would be slightly different in the wind case as indeed they would for a (more realistic) inhomogeneous fireball that could not be characterised by a single value of η . In this paper we are concerned with the intensity and spectrum of the radiation emitted near the peak; the key parameters are then η , $((E/\theta^2)$ and n_{ext} .

2.2 Shock Structure, Radiation Densities and Timescales

A crucial question is whether the radiative efficiency of the shock(s) is sufficiently high, and this depends on the magnetic field. The synchrotron radiative efficiency of the deceleration blast wave and of the reverse shock are near unity if turbulent instabilities at the shocks lead to magnetic fields not too far below equipartition. Shocks are unstable (e.g. Ryu and Vishniac, 1992), which should result in turbulence, and turbulent field growth seems to be efficient in observed supernova remnant and radio source jet shocks. Alternatively, the ejecta may be magnetically dominated, or at least contain magnetic fields which *initially* contribute a fraction ξ of the dynamical equipartition value, and subsequently remain frozen-in, so $B^2 \propto V^{-4/3}$, where V is the comoving volume. In this case the deceleration-induced reverse shock is expected to have high inverse Compton (IC) radiative efficiency (Mészáros, Laguna and Rees, 1993), for moderate values of the electron Lorentz factor. Previously, we had assumed that the IC scattering occurs on the same electrons that are responsible for the synchrotron photons, an assumption which is relaxed here. In both the turbulent generation and the frozen-in scenario, the main uncertainties are the value of the magnetic field at the deceleration radius, and the value of the typical Lorentz factor of the radiating electrons, the latter being dependent on the type of acceleration mechanism at the shock. However, under the minimal assumption that electrons are accelerated to a power law distribution, it is possible to derive reasonable lower limits to the synchrotron and IC efficiencies under various parametrizations of the field strength and the minimum electron Lorentz factor.

The detailed structure of the shocks will depend on the magnitude of the field and on the efficiency for accelerating electrons to relativistic energies. The strength and Mach number of the blast wave and the reverse shock should be different, as well as the seed field density, so in principle the field growth and acceleration efficiency could be different in both. The importance of the synchrotron and IC mechanisms will depend on the strength of the magnetic field behind the blast wave and the reverse shock, and several possible emission region configurations can be considered.

One extreme case is that where the ejecta have a frozen-in magnetic field left over from the explosion phase, at which time its energy density made up a fraction ξ of the total initial radiation density. In this case the magnetic field strength in the reverse-shocked region at the deceleration radius r_d is $B_{df} \sim 0.4\xi^{1/2}E_{51}^{-1/6}n_0^{2/3}\eta_3^2$ G. On the other hand, if the shocks are subject to instabilities, leading to magnetic field growth which reaches some fraction λ of the equipartition value with the corresponding post-shock energetic particles (as in supernova remnants, or radio sources), then the field at the deceleration radius is $B_{de} \sim 4 \times 10^2 n_0^{1/2} \eta_3 \lambda^{1/2}$ G. Notice that the equipartition (or sub-equipartition) field value is the same (if λ is the same) behind both the blast wave and the reverse shock, because the particles behind both must be in pressure equilibrium with each other. The corresponding magnetic energy densities (ergs cm⁻³) are

$$u_B \sim \begin{cases} 6.6 \times 10^3 n_0 \lambda \eta_3^2 \text{ ergs cm}^{-3}, & (\text{turbulent}); \\ 7 \times 10^{-3} n_0^{4/3} E_{51}^{-1/3} \xi \eta_3^4 \text{ ergs cm}^{-3}, & (\text{frozen-in}). \end{cases} \quad (2.2.1)$$

The parameter λ could be different in the blast wave and reverse shock (in the equipartition case), due to the different physical conditions, while the frozen-in case refers only to the reverse shock.

The acceleration mechanism is probably more efficient when the shock is strong and relativistic. Because the external medium is relatively cold and devoid of strong fields its sound speed is low, and the blast wave is certain to be strong and ultrarelativistic since the bulk Lorentz factor Γ is large. If the acceleration mechanism does not depend on the presence of fields stronger than the minimal seed field expected in the interstellar medium, an electron power law can be expected to form behind the blast wave. However the strength of any synchrotron radiation from these electrons does depend on the field strength. Thus synchrotron emission from the blast wave will be generally negligible for the fields $B \sim 10^{-6}$ G typical of normal ISM, but will be important if turbulent field growth occurs. IC scattering, however, only requires the presence of relativistic electrons, and may be expected to be important under a wide range of circumstances in the blast wave.

The reverse shock which moves into the ejecta encounters gas which is generally hotter than the external ISM, even after adiabatic cooling. For a matter-dominated fireball, the sound speed is higher and the reverse shock becomes at most marginally relativistic. Similarly, for a magnetically dominated fireball the Alfvén speed is high. However, in either case, the fireball has a large outward Lorentz factor with respect to the contact discontinuity, and the reverse shock may be strong, even if not as highly relativistic as the blast wave. Particles are plentiful in the matter-loaded fireball, and in the magnetically dominated case particles would be expected due to entrainment or due to sweeping up of neutrals from the external medium, which could be accelerated by the reverse shock. However, because both the field strength and the particle supply are different as well as the shock strength, it would not be surprising if the blast wave and reverse shock differed in their ability to accelerate particles and radiate, unless the interface were unstable and mixing occurred on short timescales.

To cover the possibilities discussed above, we consider several basic shock models. The simplest is the “frozen-in” (F) model, which assumes the existence of fields in the ejecta at some fraction ξ of the (initial) equipartition value, and no turbulent field growth in either the blast or reverse shock. Another model is the “turbulent” (T) model, where turbulent field growth is assumed to occur in both shocks leading to fields with an energy density which is a fraction λ of the particle energy in the shock (λ may be different for each shock). A third model is the “piston” (P) model, where the ejecta provides pressure but the reverse shock is assumed to be an inefficient radiator (either due to low fields or poor acceleration), while turbulent field growth and acceleration are efficient in the blast wave, which contributes all the radiation.

If a shock randomizes a large fraction of the total bulk kinetic energy, which is comparable to the initial burst energy E_o , the comoving synchrotron luminosity will be given by $L_{sy} \sim (E_o/4\pi\theta^2\eta^3)e_{sy}t_{ex}^{-1}$, where e_{sy} is the synchrotron efficiency relative to the other mechanisms (see eq.[2.3.4]). Here we used the fact that in the coasting expansion the expanding shell consists, in effect, of $\sim 4\pi\theta^2\eta^2$ causally unconnected regions,

each subtending an angle $\sim \eta^{-1}$ at the fireball's centre, and each of comoving dimension $\Delta R \sim r_d/\eta$; the comoving spectral intensity is $I_\nu \sim (L_{sy}/\nu\Delta R^2) \sim (2\nu^2/c^2)\gamma_{sy}m_e c^2$ at the frequency where self-absorption sets in. The electron Lorentz factor to be used here is $\gamma_{sy} = \max[\gamma_m, \gamma_{ab}]$, where γ_m is the minimum Lorentz factor of the electron power law produced in the shock, and $\gamma_{ab} \sim 10^{-3}B^{-1/2}\nu_{ab}^{1/2}$ is the Lorentz factor of electrons that would be radiating photons at a synchrotron frequency equal to the self-absorption frequency ν_{ab} . The comoving self-absorption frequency is therefore

$$\nu_{ab} = \left(\frac{L_{sy}c^2\eta^2}{2r_d^2\gamma_{sy}m_e c^2} \right)^{1/3} \sim \begin{cases} 7.4 \times 10^{12} n_0^{1/3} \eta_3^{2/3} (e_{sy}/\gamma_m)^{1/3}, & \text{if } \gamma_m > \gamma_{ab}; \\ 1.1 \times 10^{11} n_0^{2/7} \eta_3^{4/7} B^{1/7} (e_{sy}/10^{-3})^{2/7}, & \text{if } \gamma_m < \gamma_{ab}. \end{cases} \quad (2.2.2)$$

The value of e_{sy} and B to be used here is different for the frozen-in and turbulent cases (e.g. eq.[2.2.1]). The minimum electron Lorentz factor γ_m of the power law distribution behind a shock depends on the bulk Lorentz factor Γ , and it may exceed Γ by a factor up to $m_p/m_e \sim 10^3$. Since the reverse shock eventually becomes marginally relativistic, $(\Gamma_r - 1) \sim 1$, while the blast wave (forward) shock achieves a saturation $\Gamma_b \sim \eta$ (when $\eta < \Gamma_m \sim 3.3 \times 10^5 E_{51}^{1/3} r_6^{-2/3}$), we will parametrize the minimum electron Lorentz factor by

$$\gamma_m = \kappa\Gamma \sim \begin{cases} \kappa, & \text{(reverse shock);} \\ \kappa\eta, & \text{(blast wave),} \end{cases} \quad (2.2.3)$$

where $1 \lesssim \kappa \lesssim 10^3 \sim m_p/m_e$. The lowest energy electrons emit synchrotron photons with characteristic energy $\nu_{sy,m} \sim 10^6 B \gamma_m^2 \sim 10^6 B \kappa^2 \Gamma^2$; in the case $\kappa \sim 10^3 \kappa_3$, these are often above the self-absorption values (2.2.2).

The comoving synchrotron cooling time behind a shock characterized by $\kappa_{sy}\Gamma_{sy}$ will be

$$t_{sy} \sim \frac{3.3 \times 10^7}{\kappa_{sy}\Gamma_{sy}u_B} \sim \begin{cases} 3.1 \times 10^3 n_0^{-1} \lambda^{-1} \kappa_{sy}^{-1} \Gamma_{sy}^{-1} \eta_3^{-2} \text{ s,} & \text{(turbulent);} \\ 3.1 \times 10^9 n_0^{-4/3} E_{51}^{1/3} \xi^{-1} \kappa_{sy}^{-1} \Gamma_{sy}^{-1} \eta_3^{-4} \text{ s,} & \text{(frozen-in),} \end{cases} \quad (2.2.4)$$

which, compared to the comoving expansion time (2.1.2), can be short even for $\kappa \sim 1$ in the equipartition case, but is usually long even for $\kappa \sim 10^3$ in the frozen-in case. The synchrotron energy density can be estimated as $u_{sy} \sim n_e(4/3)\sigma_T c u_B \gamma_m^2 t_{ex}$, where the optically thin free-flight time across the region ΔR is essentially the comoving expansion time t_{ex} (2.1.2), and the electron density n_e behind *either* one of the shocks is $n_e \sim 10^6 n_0 \eta_3^2 \Gamma_{sy}^{-1}$ (since it is $10^6 n_0 \eta_3^2$ in the ejecta or reverse shock, and $10^3 n_0 \eta_3$ in the shocked external gas in the blast wave, which has $\Gamma = \Gamma_{sy} = \eta$). Thus, while u_{sy} differs in the two field cases,

$$u_{sy} \sim \begin{cases} 2 \times 10^{-1} n_0^{5/3} E_{51}^{1/3} \theta^{-2/3} \lambda \kappa_{sy}^2 \Gamma_{sy} \eta_3^{7/3} \text{ ergs cm}^{-3}, & \text{(turbulent);} \\ 2.1 \times 10^{-7} n_0^2 \theta^{-2/3} \xi \kappa_{sy}^2 \Gamma_{sy} \eta_3^{13/3} \text{ ergs cm}^{-3}, & \text{(frozen-in),} \end{cases} \quad (2.2.5)$$

the ratio

$$\frac{u_{sy}}{u_B} = 3 \times 10^{-5} n_0^{2/3} E_{51}^{1/3} \theta^{-2/3} \kappa_{sy}^2 \Gamma_{sy} \eta_3^{1/3}, \quad (2.2.6)$$

is the same in both.

The comoving IC cooling timescale is given by $t_{ic} = 3m_e c^2 / (4\sigma_t c u_{sy} \kappa_{ic} \Gamma_{ic})$, or

$$t_{ic} = 10^{12} n_0^{-2/3} E_{51}^{-1/3} \theta^{2/3} \kappa_{sy}^{-2} \kappa_{ic}^{-1} \Gamma_{sy}^{-1} \Gamma_{ic}^{-1} u_B^{-1} \eta_3^{-1/3} \\ = \begin{cases} 1.5 \times 10^8 n_0^{-5/3} E_{51}^{-1/3} \theta^{2/3} \lambda^{-1} \kappa_{sy}^{-2} \kappa_{ic}^{-2} \Gamma_{sy}^{-1} \Gamma_{ic}^{-1} \eta_3^{-7/3} \text{ s,} & (\text{turbulent}); \\ 1.4 \times 10^{14} n_0^{-2} \theta^{2/3} \xi^{-1} \kappa_{sy}^{-2} \kappa_{ic}^{-1} \Gamma_{sy}^{-1} \Gamma_{ic}^{-1} \eta_3^{-13/3} \text{ s,} & (\text{frozen-in}). \end{cases} \quad (2.2.7)$$

This includes the case when one of the shocks (with κ_{ic} , Γ_{ic}) IC-scatters synchrotron photons from the same shock or the other shock with κ_{sy} , Γ_{sy} (i.e., if synchrotron and IC occur within the same shock then $\kappa_{sy} = \kappa_{ic}$, $\Gamma_{sy} = \Gamma_{ic}$, or synchrotron and IC-scattering occur in different shocks then these quantities differ). The IC cooling timescales are, especially for the equipartition case, shorter than the comoving expansion time (2.2.2) whenever κ_{sy} or κ_{ic} are large (e.g. $\kappa \sim m_p/m_e \sim 10^3$), and even more so in the blast wave, where also $\Gamma_{sy} \sim \Gamma_{ic} \sim 10^3 \eta_3$. The ratio of the inverse Compton to the synchrotron time is

$$\frac{t_{ic}}{t_{sy}} = 4.8 \times 10^4 n_0^{-2/3} E_{51}^{-1/3} \theta^{2/3} \kappa_{sy}^{-1} \kappa_{ic}^{-1} \Gamma_{ic}^{-1} \eta_3^{-1/3}, \quad (2.2.8)$$

for both the equipartition and frozen-in cases; using ‘‘cosmological’’ parameters, this will be short for $\kappa_{sy} \kappa_{ic} \Gamma_{ic} \gtrsim 10^5$.

In the case of the blast wave, one must consider also the combined IC cooling timescale due to scattering the synchrotron photons that arise in the blast wave plus those that arise in the reverse shock and travel through the blast wave towards the observer. (Note that the bulk motion of the radiating material is only mildly relativistic with respect to the contact-discontinuity, so it is a reasonable approximation to suppose that $\sim \frac{1}{2}$ the radiation crosses the contact discontinuity). This timescale is given by $t_{ic,c} = 3m_e c^2 / [4\sigma_{TC} \kappa_{ic} \Gamma_{ic} (u_{sy,r} + u_{sy,b})]$, where $u_{sy,r}$, $u_{sy,b}$ are the synchrotron photon energy densities due to the reverse shock and blast wave respectively. Since the energy loss rates are additive, this combined IC timescale can be obtained from the appropriate combination of the timescale (2.2.8),

$$t_{ic,c}^{-1} = t_{ic,rb}^{-1} + t_{ic,bb}^{-1}, \quad (2.2.9)$$

where rb and bb stand for synchrotron/IC due to reverse/blast and blast/blast, respectively. Depending on the basic shock model being assumed, some of these components may be absent, e.g. in the piston model there are no contributions from the reverse shock, and no combined IC scattering.

2.3 Spectral Components and Fluences

The spectrum observed will be made up of a combination of one or two synchrotron spectra, and one to three IC-scattered spectra (we consider here only the case where higher order IC scattering occurs in the Klein-Nishina regime, so its contribution can be neglected relative to the others). The synchrotron spectra will be self-absorbed below ν_{ab} given by (2.2.2), in which case if $\gamma_{ab} > \gamma_m \sim \kappa\Gamma$ the synchrotron spectrum from the blast wave peaks at that frequency; the spectra have an energy slope $I_\nu \sim \nu^{s_a}$ above that, where $s_a = -(p-1)/2$ and p is the electron power law energy index above γ_m defined by $N(\gamma) \propto \gamma^{-p}$. However, in the case when $\kappa\Gamma \gg 1$ so $\gamma_m \geq \gamma_{ab}$, the negative slope $s_a = -(p-1)/2$ starts at $\nu_{sy,m} \sim 10^6 B \gamma_m^2 > \nu_{ab}$. The typical values for the non-thermal charged particle power index achieved in shock acceleration are $p \sim 2-4$, and taking an average value $p \sim 3$ leads to a synchrotron slope above the break $s_a \sim -1$. For a single field value throughout the shock emission region, the slope below this break will be $+1/3$ while the spectrum is optically thin, and $+5/2$ below ν_{ab} . In practice, however, it is unlikely that the field is uniform, and based on the analogy of compact radio sources, which show an energy slope ~ 0 below the break, one might expect also here an energy slope s_b below the break flatter than either $+1/3$ or $+2.5$. In the absence of absorption, we shall take a fiducial value of $s_b = +1/3$. The corresponding slope of the power per decade spectrum νI_ν will be $P_\nu \propto \nu^{\alpha_i} \propto \nu^{s_i+1}$ where $i = (b, a)$ for frequencies (below, above) the break. This corresponds to the ‘‘fiducial’’ values of the power slope $\alpha_b \sim +4/3$ below the break and $\alpha_a \sim 0$ above the break, close to the average values 1 and 0 (e.g. Schaefer, *et al.*, 1992) which have in the past been taken as a guideline. However, one must be aware of the fact that there is a considerable spread about these values (e.g., Band, *et al.*, 1993).

The lab-frame frequency of the synchrotron break or turnover will be given either by the comoving self-absorption frequency (2.2.2), or (for the larger $\kappa_{sy}\Gamma_{sy}$ in either shock) by $\nu_{sy,m} \sim 10^6 B \gamma_m^2$, in both cases blueshifted by $\eta = 10^3 \eta_3$ (the bulk Lorentz factor of both the reverse shock and the blast wave, in the observer frame). In the latter case, the lab-frame synchrotron turnover frequency is

$$\nu_{syt} \simeq \begin{cases} 4 \times 10^{11} n_0^{1/2} \lambda^{1/2} \kappa_{sy}^2 \Gamma_{sy}^2 \eta_3^2 \text{ Hz}, & (\text{turbulent}); \\ 4 \times 10^8 n_0^{2/3} E_{51}^{-1/6} r_6^{1/2} \xi^{1/2} \kappa_{sy}^2 \Gamma_{sy}^2 \eta_3^3 \text{ Hz}, & (\text{frozen-in}), \end{cases} \quad (2.3.1)$$

The IC-scattered spectrum will show a corresponding IC break or turnover at a lab-frame frequency $\nu_{ict} \sim (4/3) \kappa_{ic}^2 \Gamma_{ic}^2 \nu_{syt} \sim 1.3 \times 10^9 B \kappa_{sy}^2 \kappa_{ic}^2 \Gamma_{sy}^2 \Gamma_{ic}^2 \eta_3$, or

$$\nu_{ict} \simeq \begin{cases} 5.3 \times 10^{11} n_0^{1/2} \lambda^{1/2} \kappa_{sy}^2 \kappa_{ic}^2 \Gamma_{sy}^2 \Gamma_{ic}^2 \eta_3^2 \text{ Hz}, & (\text{turbulent}); \\ 5.3 \times 10^8 n_0^{2/3} E_{51}^{-1/6} r_6^{1/2} \xi^{1/2} \kappa_{sy}^2 \kappa_{ic}^2 \Gamma_{sy}^2 \Gamma_{ic}^2 \eta_3^3 \text{ Hz}, & (\text{frozen-in}). \end{cases} \quad (2.3.2)$$

The IC-continuum slope below the turnover will be the same as for the synchrotron spectrum, and that above the turnover will also be the same as long as the electron slope of the IC-scattering electrons p_{ic} is even slightly steeper than that of the of the synchrotron electrons p_{sy} , in the case of scattering of reverse-shock photons on blast wave electrons. If

the synchrotron and IC electron slopes are the same, the IC slope above the turnover is logarithmically flatter than that of the synchrotron spectrum. This logarithmic flattening, if present, will be ignored below, since it does not affect substantially the discussion. Alternatively, if the synchrotron electrons have a slope p_{sy} steeper than p_{ic} , the IC-scattered photon energy spectrum has a slope of $-(p_{ic} - 1)/2$, which we will take for numerical examples to be of order -1 (corresponding to a power per decade or fluence per decade slope $\alpha_a = 0$).

The total spectrum will then show a number of spectral components due to the various synchrotron and IC combinations possible between the two shocks, compatible with the assumptions made about the field origin. In the simpler case of frozen-in magnetic fields in the ejecta, which will affect only the reverse shock (and assuming that turbulent magnetic field generation in both shocks is inefficient, $\lambda \ll 1$), we have three components: one synchrotron from the reverse shock, and two IC, one from the reverse and one from the blast wave. These may be labeled (sy, r) , (ic, rr) , (ic, rb) . In the case where turbulent field generation is efficient enough to achieve a non-negligible fraction of the equipartition magnetic field value in both shocks (i.e., a field larger than whatever frozen-in component that may be present) there are five spectral components: two synchrotron, one from each shock, and three IC. These may be labelled (sy, r) , (sy, b) , (ic, rr) , (ic, bb) , (ic, rb) . Intermediate situations may exist if turbulent field generation is efficient in only one shock but not the other, which can be treated in a similar manner.

Each spectral component will produce a total photon energy fluence S (ergs cm⁻²), which is some fraction $\lesssim 1$ of the maximum bolometric fluence available from the particular shock in question. In the most common case when $\eta < \Gamma_m = 3.3 \times 10^5 E_{51}^{1/3} r_6^{-2/3}$, most of the initial fireball energy is carried as kinetic energy of motion of the ejecta, which is completely re-randomized in the blast wave and the reverse shock. We shall therefore assume that the maximum bolometric fluence possible $S_o = S_r + S_b$ is divided about equally between the reverse shock and the blast wave, and is

$$S_o = (\varepsilon_r + \varepsilon_b)(S_o/2) = E_o/4\pi\theta^2 D_L^2 = 10^{-6} E_{51} \theta^{-2} D_{28}^{-2} \text{ ergs cm}^{-2}, \quad (2.3.3)$$

where $\varepsilon_r \sim 1$, $\varepsilon_b \sim 1$ are parameters describing what fraction of the total bolometric fluence is carried by the reverse and blast wave shocks, and D_L is the luminosity distance, $D_L = (2c/H_o)[(1+z) - (1+z)^{1/2}] \sim 10^{28} h^{-1}$ for $z \sim 1$ in an Einstein-de Sitter universe, or its appropriate Newtonian scaling for galactic models.

For each shock we can define the synchrotron and IC radiative efficiencies e_{sy} , e_{ic} for individual spectral components as

$$e_{ic} = \frac{t_{ic}^{-1}}{t_{ic}^{-1} + t_{sy}^{-1} + t_{ex}^{-1}}, \quad e_{sy} = \frac{t_{sy}^{-1}}{t_{ic}^{-1} + t_{sy}^{-1} + t_{ex}^{-1}}, \quad (2.3.4)$$

where the energy-loss timescales have to be evaluated for the particular shock j and the particular spectral component (combination of shocks j, k), e.g. in the IC case, one could

have $t_{ic,rr}$, $t_{ic,bb}$ or $t_{ic,rb}$. The corresponding photon energy fluences from each shock or shock combination due to each mechanism (giving the different spectral component) are

$$S_{ic,jk} = \varepsilon_j(S_o/2)e_{ic,jk} \quad , \quad S_{sy,j} = \varepsilon_j(S_o/2)e_{sy,j} \quad , \quad (2.3.5)$$

each extending over an energy range that goes significantly below and above the turnover (break), to an extent depending on the upper and lower limits of the electron energies.

2.4 Gamma-ray, X-ray and Optical Fluences.

We consider now more specifically the fluences in three frequency bands $\Delta\nu/\nu \sim 1$ centered around 1.2×10^{20} Hz (γ -rays near 0.5 MeV), 3×10^{17} Hz (medium/soft X-rays) and 10^{15} Hz (O/UV), matching approximately the HETE instrument bands (Ricker, 1992). We take the synchrotron spectrum to be given by a broken power law in energy flux, $I_\nu \sim \nu^{s_i}$, where $s_i = [s_b, s_a]$ for $\nu <> \nu_{syt}$, in terms of the observed lab-frame ν_{syt} of eq. (2.3.1-2.3.2). The IC-scattered spectrum will also be a broken power law with the same energy indices, $I_\nu \propto \nu^{s_i}$, while the corresponding power per decade (and fluence per decade) spectra have slopes $P_\nu = \nu I_\nu \propto \nu^{\alpha_i}$ where $\alpha_i = s_i + 1$. In a double-logarithmic plot the IC spectrum is shifted with respect to the synchrotron spectrum upwards and to the right by a factor $(4/3)\kappa^2\Gamma^2$. (We assumed, for simplicity, that the scattering electron energy index p satisfies $s_a \lesssim (p-1)/2$, although this is not necessary). The γ -ray fluence in the $\nu \sim \nu_\gamma \simeq 0.5$ MeV band will then be given by the sum (or in practice by the largest) of the various IC and synchrotron spectral contributions in that band. If self-absorption effects can be ignored, this is

$$S_\gamma = \sum_{n,jk} A_{n,jk} S_{n,jk} (\nu_\gamma/\nu_{nt,jk})^{\alpha_i} \quad \text{ergs cm}^{-2} \quad (2.4.1)$$

where n stands for synchrotron or IC, nt stands for the turnover syt or ict , jk stands for the shock combinations rr , bb or rb (where relevant), the constant $A_{n,jk} \sim 1/\text{few}$ is taken for numerical estimates to be $A = 0.2$, and $\nu_{nt,jk}$ stands for the n -mechanism turnover frequency of the shock combination jk . Similarly the X-ray fluence in the $\nu \sim \nu_x \simeq 3$ keV band is given by

$$S_x = \sum_{n,jk} A_{n,jk} S_{n,jk} (\nu_x/\nu_{nt,jk})^{\alpha_i} \quad \text{ergs cm}^{-2} \quad (2.4.2)$$

and the O/UV fluence in the $\nu \sim \nu_u \simeq 10^{15}$ Hz band is given by

$$S_u = \sum_{n,jk} A_{n,jk} S_{n,jk} (\nu_u/\nu_{nt,jk})^{\alpha_i} \quad \text{ergs cm}^{-2} \quad (2.4.3)$$

The above are without self-absorption, and generally we take $\alpha_b, \alpha_a = 4/3, 0$, although observationally other values are also expected. However, in many cases the spectra are more complicated than (2.4.1-2.4.3) because self-absorption becomes important at the

lower energies. For $\nu_{ab} < \nu_m$, the slope is α_a for $\nu > \nu_m$, it is α_b ($\sim 4/3$) for $\nu_{ab} < \nu < \nu_m$, and 3 for $\nu < \nu_{ab}$ (e.g. 0, $4/3$, 3 for decreasing energies). For $\nu_{ab} > \nu_m$, it is α_a for $\nu > \nu_{ab}$, it is 3.5 for $\nu_m < \nu < \nu_{ab}$, and 3 for $\nu < \nu_m$ (e.g. 0, 3.5, 3 for decreasing energies). In these cases, an individual synchrotron component has two breaks, and the corresponding IC-scattered component will also reflect this fact. Notice that the power in a certain band (e.g. eqs. 2.4.1-2.4.3) depends on the slopes α_i , but the power at the break energies $S_{n,jk}$ (eq. 2.3.5) is independent of these slopes. Thus, unless the bands are very far from the break energies and the slopes are very different from those assumed here, the band fluences should not be too different from those estimated with the fiducial slopes $4/3$, 0. The limiting γ -ray sensitivity of BATSE (e.g. Fishman, 1992) is $S_\gamma \sim 10^{-8}$ ergs cm $^{-2}$, while for bursts of 10 s that of HETE (Ricker, 1992) is $S_\gamma \sim 3 \times 10^{-7}$ ergs cm $^{-2}$, and in the X-ray and UV bands the sensitivity limits are $S_x \sim 8 \times 10^{-8}$ ergs cm $^{-2}$ and $S_u \sim 10^{-8}$ ergs cm $^{-2}$.

The calculated positions of the spectral breaks, and the slopes of the power-law segments of the spectra, are shown in the figures. In these figures, the breaks are depicted as being sharp. In reality they will be smoother, not only because an individual electron emits broad-band radiation but also because the observed flux comes from different parts of the fireball whose doppler shifts have a spread of order 2 (from $\sim \eta$ to almost 2η).

3. Results

3.1.1 General Features

In general the fluences scale as D^{-2} , and as a positive power (usually not unity, due to the efficiency factors) of the intrinsic total initial energy E_o . They also scale as a negative power of the beaming half-angle θ , which is generally not θ^{-2} (again due to the θ dependence of the efficiency and turnover factors). The fluences also scale as a positive power of the external density n_0 , generally between $1/3$ and $2/3$. They also depend on η ; it is the burst timescale, however, which is the most sensitive to this parameter.

In the cosmological case we adopt $E_o = 10^{51} E_{51}$ ergs and $D = 10^{28} D_{28}$ cm. For $n_0 = 1$ the burst duration for $\eta_3 = 1$ is $t_L = 5$ s and the maximum photon bolometric fluence is $S_m \sim 10^{-6} E_{51} D^{-2} \theta^{-2} e_t$, where e_t is the total radiative efficiency which depends (usually nonlinearly) on E_{51}, n_0 , etc. For smaller η and/or smaller n_0 the observed timescale gets longer, and vice versa.

In the galactic halo case we use, e.g., $E_o = 10^{41}$ ergs, $D = 1.5 \times 10^{23}$ cm = 50 kpc, while for the galactic disk we use generally $E_o = 10^{39}$ ergs, $D = 3 \times 10^{21}$ cm = 1 kpc. The maximum bolometric fluences S_m are (in principle) similar to the cosmological case, for this choice. However, especially in the frozen-in field models, which are inefficient radiators, higher E_o are occasionally needed to reproduce the observed γ -ray band fluences. Compared to the cosmological case, the durations are comparable for the halo (where typically $n_0 = 10^{-3}$), but for the galactic disk (where typically $n_0 = 1$) they are shorter (see eq.2.1.4). The typical external densities are the interstellar values expected for the

halo/disk case, unless the burst occurs inside a denser pocket of material, e.g. a wind or nebula that preceded the event. For the lowest interstellar densities, acceptable γ -ray fluences require generally large $\kappa \sim 10^3$, while for higher densities $n_0 \gtrsim 1$ $\kappa \gtrsim 40$ is required.

The spectrum depends on the value of κ and λ in the shocks, and we generally assume that κ and λ are the same (or do not differ much) for both shocks. We shall consider values of $10^{-6} \lesssim (\lambda, \xi) \lesssim 1$, $10^{-3} \lesssim n_0 \lesssim 10^3$, $\kappa = 1, 40, 10^3$, $1 \lesssim \eta \lesssim 10^4$ and slopes $\alpha_i = 4/3, 0$ in most of the illustrative cases discussed below.

3.1.2 Frozen-in Field Models (F)

In this model magnetic fields are assumed to have built up in the ejecta at the beginning of the fireball's history to some fraction ξ of the equipartition value with the total initial disposable energy E_o . Magnetic fields in the blast wave and reverse shock due to turbulence, etc., are assumed to be weak, so that synchrotron radiation is important only in the reverse shock, where the frozen-in field is characterized by ξ , but IC scattering in the blast wave is important, because it efficiently accelerates electrons to high γ . This scenario has only three radiation components. It is also the least efficient, the synchrotron and IC radiative efficiencies being generally smaller for $\xi = 1$ than for the $\lambda = 1$ shock-turbulent or piston models with the same external density (which we discuss below). This is because $\xi = 1$ means equipartition at the original explosion, but then the field energy decreases adiabatically with the expansion; even after compression (by a modest factor) in the reverse shock, it is well below equipartition with the bulk kinetic energy (see eq. 2.2.1).

At cosmological distances, if one uses the low value $\kappa = 1$ in both shocks, and $\theta = \xi = 1$, the fluences in all three wavebands are below the detection threshold for $D_{28} = 1$, and are of course smaller for $\xi < 1$. However the situation is better for the case when $\kappa \gg 1$, especially if the burst is beamed. For $\theta = 10^{-1}$, $\kappa = 10^3$ and $n_0 = \xi = 1$, the γ -ray fluences are well above threshold, and the major break is in the neighborhood of the γ -ray band, so that the X-ray fluence is significantly lower, for a range of burst durations comparable to that in observed GRBs. A spectrum for this frozen cosmological (FC) model is shown in Fig. 1a, where the individual components are also indicated. The frozen-in models are easily detectable up to $D_{28} \lesssim 1$ for values of ξ not too far below unity. For the same parameters but $\xi \lesssim 10^{-2}$ the γ -ray fluences would drop below detectability, unless $D_{28} \lesssim 10^{-1}$ or the external medium is denser. For instance, $\xi = 10^{-3}$, $n_0 = 10^3$, $D_{28} = 1$ yields large γ -ray fluences and reasonable X-ray fluences.

At galactic halo and galactic disk distances, because of the lower total energy, the deceleration radii r_d are generally smaller. A burst of given duration requires a smaller η (for a given n_{ext}). The magnetic fields are weaker, and the cooling times are longer while the comoving expansion time is shorter. Therefore the efficiencies are lower than in the cosmological case, and their relative values change. Thus, in the galactic cases the synchrotron efficiency generally exceeds the IC efficiency, even for large values of $\kappa \sim 10^3$ (unless the burst occurs inside very dense clouds $n_0 \gtrsim 10^6 \text{ cm}^{-3}$). The spectra are

consequently different from those of the same model at cosmological distances. Because of the intrinsically lower radiative efficiency of the frozen-in models (compared to the turbulent and piston models), detectable fluences are obtained only for relatively large (by galactic standards) total burst energies, e.g. $E_o = 10^{45}$ ergs and higher for the halo or $E_o = 10^{43}$ ergs for the disk. Acceptable γ -ray fluences are obtained mainly for beamed, high κ cases, e.g. $\theta = 10^{-1}$, $\kappa = 10^3$ and $\xi = 1$. A spectrum for the frozen halo (FH) case is shown in Fig. 2a, for these parameters, $n_0 = 10^{-3}$ and two values of η corresponding to 12 s and 0.5 s durations. A spectrum for the frozen galactic disk (FD) case ($n_0 = 1$) is given in Fig. 3a, for 5 s and 0.25 s. In both halo and disk cases the major break is below all three observational bands, so the fluences at UV, X-rays and γ -rays are all comparable, $S_x/S_\gamma \sim S_u/S_\gamma \sim 1$.

The general behavior of the spectra for bursts of various durations is shown, for the frozen-in cosmological (FC) model in Fig. 4, for the same parameters as Fig. 1a but variable duration t_L . The three break energies tend to be softer for the longer total durations, and also the fluence levels within the same plateau are smaller for longer durations. However, for a fixed energy band the fluence can also increase rather steeply as the duration is taken longer, if one of the breaks moves across that energy band.

3.1.3 Turbulent Field Growth Models (T)

In this model turbulent magnetic fields are assumed to build up to some fraction λ of the equipartition value in both the reverse and blast wave shocks (not necessarily the same in both, although here we assumed them to be equal). As a result there are generally five different spectral components, although often one component dominates over several of the bands γ, x, u . For values of $\kappa \sim 1$ in both shocks, i.e. $\gamma_m \sim \Gamma$, the synchrotron efficiency is generally larger than that for the IC process. For larger κ the importance of IC is larger, and in the cosmological case (where E_o is larger so r_d is larger and B_d smaller) it dominates the radiative efficiency. At galactic distances, E_o and B_d are smaller and synchrotron remains mostly dominant, even when IC is important from the spectral point of view.

For cosmological distances, observable γ -ray fluences are obtained for $\kappa = 1$ if $\lambda \gtrsim 10^{-3}$, and for $\kappa \sim 10^3$ even for values λ well below 10^{-6} . However, for $\lambda \gg 10^{-6}$ this model is also extremely efficient in producing radiation at other frequencies below the γ -ray band. A turbulent cosmological (TC) spectrum for standard parameters $n_0 = 1$, $\kappa = 10^3$, $\lambda = 10^{-6}$, $\theta = 10^{-1}$, $\eta_3 = 1$, $t_L = 5$ s is given in Fig. 1b, showing the five spectral components. It is seen that, even for this low field case (10^{-6} of the equipartition value) the γ -ray fluence is high. This is true also for higher λ values, but the X-ray to γ -ray fluence ratio S_x/S_γ is then closer to unity, whereas for the lower values such as $\lambda = 10^{-6}$ this ratio is of order $\lesssim 0.03$. It is worth noting that the spectrum for the frozen-in model with $\xi = 1$ plotted in Fig. 1a is essentially the same as that for the ‘‘turbulent’’ model at the same distance with $\lambda = 10^{-6}$ (in Fig. 1b). The reason for this is that for this choice of λ and ξ the fields in the shock at deceleration have the same magnitude (eqs. 2.2.1), so

the dominant reverse-shock synchrotron, reverse-shock IC and blast wave combined IC are the same, while the blast wave synchrotron and blast wave IC spectra are below the other three components.

For galactic halo and disk distances the turbulent model γ -ray fluence is generally high, even for densities somewhat lower than the standard interstellar values ($n_0 = 10^{-3}$ halo, $n_0 = 1$ disk), especially at the higher κ values. As in the galactic frozen-in models, due to the lower field value the breaks occur at relatively low energies and the flat (slope 0) spectrum extends to energies lower than in the cosmological case. As a result, there is an increased tendency to produce a relatively large X-ray fluence, both the γ - and X-ray bands falling above the main break. There are some exceptions to this situation, e.g. in the disk case for $\theta = 10^{-1}$, $\lambda = 10^{-3}$, $\kappa = 10^3$ the X-ray fluence is well below the γ -ray fluence for short bursts $\eta = 10^2$, $t_L = 0.2$ s, but they are comparable for the longer bursts $t_L \gtrsim 1$ s, and for longer bursts the UV fluence can also be significant. The spectra characteristic of such short and long duration halo and galactic disk turbulent models are shown in Figs. 2b and 3b.

The spectra of bursts as a function of burst duration is shown for the turbulent cosmological model TC in Fig. 5, for fields in the shock which are $\lambda = 10^{-6}$ below equipartition. These spectra show the same break softening and plateau fluence decrease with increasing duration as seen in the frozen-in case, but less pronounced. The reason for the difference is the different η dependence (or t_L dependence) of the field B at the shock (eq. 2.2.1). For this choice of $\xi = 1$ (frozen) and $\lambda = 10^{-6}$ (turbulent) the fields (and spectra) are the same at $t_L = 5$ s ($\eta = 10^3$), but differ at other durations (other η). For this low λ , the two additional spectral components in the turbulent model just begin to become noticeable at the longest durations. The two lower energy breaks are due to the reverse shock synchrotron and IC, while the two highest are the blast wave self-IC and combined IC (the blast wave synchrotron is just visible around 10^3 s near 10^{17} Hz). The MeV band is in the neighborhood of the reverse IC component (redshift is not included in the cosmological plots shown).

In Fig. 6 we show the turbulent halo model spectra as a function of duration. In this case the two main breaks are the reverse and blast synchrotron breaks, the MeV band falling near the blast synchrotron break. The turbulent galactic disk model is similar, but the MeV band is farther up on the plateau above the blast synchrotron break, while the reverse synchrotron is closer in fluence and energy to the blast synchrotron component.

3.1.4 Piston Models (P)

The physics of these models is the same as in the turbulent field growth cases discussed before, except that there are no radiative contributions from the reverse shock, only from the blast wave. The spectra have only two components, synchrotron and IC. The relative importance of the blast synchrotron and IC contributions are changed, relative to the two-shock turbulent growth model, because the much more abundant reverse shock photons which previously acted as seeds for the blast wave IC are now absent. For this reason, the

blast wave synchrotron spectrum dominates in almost all cases. The spectrum being so simple, the value of the fluence at each band is determined simply by the slopes assumed and by whether the observed band is above or below the synchrotron break. It is therefore strongly dependent on the field strength λ and the particle minimum energy κ .

The cosmological piston (PC) model has a high bolometric radiative efficiency for a wide range of λ and κ . The highest γ -ray fluences (for a slope 0 above the break) are obtained when the break is below the γ -band, which requires λ and/or κ not to be too large. Values of $\kappa \sim 10^3$ are too large, but high γ -fluences are obtained for $\kappa \lesssim 10^2$, for a range of burst durations. When κ is much lower than this, and/or λ is very low, the X-ray fluence can become comparable to the γ -ray fluence. The spectrum of a cosmological piston model and its components is shown in Fig. 1c.

The piston models in the halo and galactic disk (PH, PD) have a lower radiative efficiency than the cosmological piston case, due to the lower energy density and corresponding lower magnetic field in the blast wave. The total energies required to obtain acceptable γ -ray fluences are comparable to those in the turbulent growth model, $E_o = 10^{41}$ ergs (halo) and $E_o = 10^{39}$ ergs (disk). Due to the lower field the break energy appears at low frequencies, typically below the UV band. High bolometric fluences are obtained for large $\kappa \sim 10^3$, giving spectra whose fluences in the γ -ray and X-ray bands are comparable for a high energy slope of 0 for durations $t_L \gtrsim 1$ s, but ratios $S_x/S_\gamma \lesssim 0.03$ are obtained in the short bursts ($t_L \lesssim 1$ s).

In Fig. 7 we show, for a fixed density, the piston cosmological (PC) spectra expected as a function of the burst duration, for $\lambda = 10^{-3}$. The piston models have only blast wave spectral components, and in this case the MeV band falls near the blast synchrotron break, while the blast IC component is seen at the highest energies.

In Fig. 8 the piston disk case (PD) is shown, where again the MeV band falls nearest to the blast synchrotron break, while the blast IC component is not sufficiently strong to show up. The corresponding piston halo model shows similar properties.

3.1.5 Gamma-ray and X-ray Fluences

The spectra previously discussed refer to 'standard' densities, and it is interesting to consider other values as well. In the density-duration parameter space, we have calculated the γ -ray band S_γ fluence contour levels and also the ratio S_γ/S_x , these two bands being centered around 0.5 MeV and 1 KeV. These are the most likely to be of immediate use in constraining models. Similar contour levels for the S_γ/S_u ratio can also be made but are omitted here for brevity. The S_γ contours start at the approximate BATSE threshold of 10^{-8} ergs cm^{-2} and higher values, while the S_γ/S_x contours go from 1 to 10^2 . Of course, other values also occur, but these delimit the most interesting range between comparable γ to X-ray ratio and the usual "X-ray paucity" value of $S_x/S_\gamma \lesssim$ few percent. For each model these two sets of contours are shown simultaneously in Fig. 9. The left column shows the cosmological models (frozen, turbulent and piston from top to bottom), the middle column the halo models and the right column the galactic disk models (same distribution).

The frozen and turbulent cosmological S_γ and S_γ/S_x contours behave fairly similarly in the n, t_L plane, not surprisingly since the field values were chosen approximately similar. The higher fluences are in the $n \gtrsim 1$, $t_L \gtrsim 5$ s upper right quadrant, but detectable S_γ is obtained over much of the range $10^{-1} \lesssim t_L \lesssim 10^3$, $10^{-3} \lesssim n \lesssim 10^3$. The region where the S_γ/S_x ratio is larger than 30 is also in the upper right quadrant, so longer bursts are better at satisfying the X-ray paucity constraint. The cosmological piston contours are much simpler, due to the simpler (essentially one component) structure: burst in a medium of $n \lesssim 10^2$ and with $t_L \gtrsim 1$ s are all above threshold, and those at all densities with $t_L \lesssim 12$ s satisfy a gamma/X ratio $\gtrsim 30$. Here it is the short bursts that satisfy X-ray paucity. This difference between frozen/turbulent and piston is due to the fact that, for this particular choice of λ, ξ and κ the former have the γ band halfway up the break slope, while the latter has it on the plateau above the break, and the break softens with increasing duration. The details of the behavior, it must be stressed, are a function of the choice of parameters.

For the halo models (middle column of Fig. 9) the frozen models are above γ threshold everywhere except at long durations and low densities, higher S_γ occurring for shorter durations and higher densities. For the frozen model the X-ray paucity ratio of 30 is violated almost everywhere, while gamma/x ratios $\gtrsim 10$ are obtained for $t_L \gtrsim 5$ s, $n \gtrsim 10^2$. The turbulent and piston halo are above γ -threshold essentially everywhere, but turbulent satisfies a gamma/x ratio $\gtrsim 30$ for $n \lesssim 10^{-2}$ and durations 0.2 s $\lesssim t_L \lesssim 5$ s, while the piston does it for all densities and $t_L \lesssim 5$ s.

For galactic disk models (right column) the frozen models behave similarly to the halo case (middle column), but the region where the gamma/x ratio is larger than 10 is smaller ($n_0 \gtrsim 10^2$, $10^2 \lesssim n \lesssim 10^3$). The turbulent disk has a somewhat larger region in the low density, short time quadrant where this ratio $\gtrsim 10$ is satisfied, and the piston disk satisfies it for all densities and $t_L \lesssim 1$ s.

Also shown in Fig. 9 are the lines below which impulsive bursts are not possible, shown as full straight lines running diagonally from top left to bottom right in the halo and galactic disk cases. In the cosmological cases these lines are outside the figures for the range of values used, so this restriction does not apply. Short bursts below and to the left of this line would require, in the impulsive burst limit (energy deposition time \ll burst duration t_L), a value of $\Gamma = \eta$ which exceeds the maximum value compatible with dynamical requirements, $\eta > \Gamma_m = 3.3 \times 10^2 E_{42}^{1/3} r_6^{-2/3}$ (e.g. Mészáros, Laguna and Rees, 1993). Bursts below this line, therefore, are only consistent with an interpretation where the timescale t_L is not given by the dynamics as a function of η , via eq.(2.1.4) (see also below).

4. Discussion

We have calculated the radiation spectra of gamma-ray burst sources arising in the blast wave produced when relativistic ejecta encounter the external medium. While there are a number of uncertainties concerning the field strength and the particle acceleration efficiency in the blast wave and reverse shocks, a simple parametrization has been used to determine the range of physical conditions that can be encountered. For models where turbulent magnetic field growth occurs in the shock the field strength is characterized by λ , which is the ratio of the magnetic to the particle energy in the shock, while frozen-in fields are characterized by ξ , which is the corresponding ratio at the time of the initial impulsive event. The particle acceleration is characterized by the ratio κ of the minimum electron Lorentz factor in units of the bulk Lorentz factor of the burst. The range of parameters explored is that which reproduces the observed gamma-ray fluences and the overall burst durations, 10^{-8} ergs cm $^{-2}$ \lesssim $S_\gamma \lesssim 10^{-4}$ ergs cm $^{-2}$ and 10^{-1} s \lesssim $t_L \lesssim 10^3$ s. Temporal substructure on shorter timescales is expected, since the external medium is likely to be lumpy and the shocks are expected to be unstable. These gross features of GRBs are easily explained by the impulsive energy deposition model with physically reasonable values of these parameters, within the context of the models discussed here.

A natural explanation for the non-thermal, power-law spectrum seen in the bursts in the gamma-ray range is provided by the synchrotron and inverse Compton radiation losses expected from the power law relativistic electrons accelerated in the shocks. Also the presence of breaks by about one unit in the power law finds a natural explanation in this model. These are associated with the minimum energy to which relativistic electrons are accelerated. Steeper breaks can also arise from synchrotron self-absorption, which we have evaluated here for the case of relativistically expanding sources. This is important in some cases, but it appears usually below the UV range.

The breaks do not appear at a preferred energy, the latter depending on the parameter η and external density as well as κ . For a fixed assumed fraction of the equipartition energy density λ , the magnetic field at the shocks depends on η and the break energies depend on B and powers of Γ . Since for the reverse shock Γ_r is always of order unity, the blast wave $\Gamma_b = \eta$, the η (or t_L) dependence of the break energy is stronger for the blast wave components than for the reverse components. The softening of the ‘main’ piston spectral break (due to the blast wave) with decreasing η (increasing baryon loading, or increasing burst duration t_L) is more pronounced than the softening of the ‘main’ break (due to the reverse shock) in the turbulent and frozen-in models, but it is comparable to the softening of the third, combined IC break (due to the blast wave) in these models.

Specific constraints are obtained by comparing the fluence in different parts of the spectrum. In particular, the usually invoked X-ray paucity constraint $S_x/S_\gamma \lesssim 0.03$ (e.g. Laros, *et al.*, 1984), if applied universally, provides stringent restrictions on the type of models which are acceptable. Only the cosmological models are able to satisfy this condition over the entire range of durations 120^{-1} s \lesssim $t_L \lesssim 10^3$ s: turbulent cosmological models are satisfactory for relatively low values of $\lambda \lesssim 10^{-6}$, piston cosmological models are satisfactory over a wide range of values of λ , and frozen-in cosmological models require

relatively high values of $\xi \gtrsim 10^{-1}$. On the other hand, the galactic models produce lower magnetic fields in the shocks, and a direct consequence of this is that their breaks occur generally at energies below the X-ray band. This holds for impulsive bursts, where t_L is determined by $\eta < \Gamma_m = 3.3 \times 10^5 E_{51}^{1/3} r_6^{-2/3}$ (eq.2.1.4), for durations $t_L \gtrsim 1$ s. Galactic models would therefore not produce γ -ray breaks, and would also predict rather high $S_x/S_\gamma \sim L_x/L_\gamma \sim 1$ fluence ratios violating the X-ray paucity ratio as defined above, except for very short bursts with (impulsive) duration $t_L \lesssim 1$ s given by eq.(2.1.4). A possible way around this might be if the bursts are not impulsive, i.e. the original energy input has an intrinsic, longer timescale which is identified as the burst duration, e.g. it is t_w for a wind model, or t_{accr} for an accretion model. In Fig. 9, impulsive models can only exist above and to the right of the diagonal solid line (in the cosmological models, this line is outside the figure boundaries). Below this line, in halo and galactic disk models, only non-impulsive models are allowed, where η and the duration are independent parameters not connected by eq.(2.1.4). The duration could, in this case, be given, e.g., by the wind duration t_w discussed in §2.1, or by an accretion time t_{acc} . For non-impulsive models, in Figs. 1 through 9, the duration (t_L) values plotted would not be the real duration; the “duration” values in Figs. 4-9 can, however, be simply re-interpreted as a quantity proportional to an inverse power of $\eta = E_o/M_o c^2$, a characteristic of the model, while the real duration is an extra model parameter. The cosmological models, however, can satisfy the impulsive approximation throughout the region of parameter space here considered, so for these the duration t_L of eq.(2.1.4) can be self-consistently determined from η . (Non-impulsive models could also be considered in the cosmological case, at the price of introducing a model-dependent timescale, but this is not necessary).

There is a well-defined density dependence of the fluences, as seen from Figs 1d, 2d and 3d for the piston model (this holds also for the other two models). The reason for this is that the deceleration radius (2.1.1) depends on density, and this determines both the duration (2.1.4) of the burst and the field strength (2.2.1) at the shock. While the break energy behaves monotonically with n_0 , the fluence does not, since that depends on the ratio of synchrotron to IC efficiencies which is a more complicated function of the density. The density effect is also seen in Fig. 9, where the lines of $S_\gamma = \text{constant}$ and $S_\gamma/S_x = \text{constant}$ are plotted in the n_o, t_L plane. This defines the regions where both an “X-ray paucity” constraint and a minimum γ -ray fluence constraint can be satisfied for the three models considered, in both the galactic and cosmological cases and for various values of the field generation parameter ξ (or λ) and the particle acceleration parameter κ . It is seen that, in general, an external density $n_o \gtrsim 1 \text{ cm}^{-3}$ is required to produce acceptable fluences. This would be an argument against having GRB in a galactic halo. In the case of GRB in our galactic disk it would predict that they are seen only inside spiral arms, where the ISM density is the standard value $n_o \sim 1 \text{ cm}^{-3}$ or greater (but the X-ray paucity constraint and burst duration constraint cannot be easily satisfied, unless additional assumptions are made, as discussed above). Strong γ emission could arise if the electron spectrum were flatter (with $p < 3$), so that synchrotron emission from the highest-energy electrons was the dominant process (cf. Begelman *et al.* 1993). In the case of cosmological bursts, Figure 9 suggest that the GRB occur in (distant) spiral galaxies or other “galactic” environments where the density is of the order or above the standard ISM

density of 1 cm^{-3} . However, it is possible that cosmological GRB which have wandered out of their host galaxy, or galactic GRB in a halo, could be inside a “local high density pocket” produced, e.g. by a precursor wind, and might therefore have fluences comparable to those of bursts in a high density ISM.

The spectral calculations are used also to make predictions of the optical/UV and the GeV/TeV fluences, as well as the X-ray fluences expected from bursts with a given MeV-band fluence and duration. These fluences can be compared with the limiting sensitivities of BATSE (e.g. Fishman, 1992) $S_{\gamma,m} \sim 10^{-8} \text{ ergs cm}^{-2}$ in the γ -ray band, and of HETE (Ricker, 1992), $S_{\gamma,m}/t_L \sim 3 \times 10^{-8} \text{ ergs cm}^{-2} \text{ s}^{-1}$, $S_{x,m}/t_L \sim 8 \times 10^{-9} \text{ ergs cm}^{-2} \text{ s}^{-1}$ and $S_{u,m}/t_L \sim 10^{-9} \text{ ergs cm}^{-2} \text{ s}^{-1}$ in the γ -ray, X-ray and O/UV bands respectively (10σ limits). For a typical burst duration $t_L \sim 10 \text{ s}$, the HETE fluence sensitivity limits are $S_{\gamma} \sim 3 \times 10^{-7} \text{ ergs cm}^{-2}$, $S_x \sim 8 \times 10^{-8} \text{ ergs cm}^{-2}$ and $S_u \sim 10^{-8} \text{ ergs cm}^{-2}$.

Significant X-ray fluences are predicted in some of the models. For a given (observable) γ -ray fluence, even if one imposes restrictions on the model parameters to satisfy an X-ray paucity constraint (e.g., based on current observations, $S_x/S_{\gamma} \lesssim 3 \times 10^{-2}$), the models predict X-ray fluences that ought to be detectable. With current detectors this is possible *if* the GRB happens to be in the (usually rather narrow) X-ray detector field of view. The latter, unfortunately, is statistically improbable. For instance, the Rosat field of view is 3 square degrees, i.e. $\sim 10^{-4}$ of the entire sky, so for a burst rate of one per day, one would have to wait $\sim 10^4$ days to find a GRB in the field of view. This situation, however, should greatly improve with the advent of a new generation of omnidirectional X-ray detectors, e.g. HETE (Ricker, *et al.*, 1993). The predicted X-ray fluences, even when satisfying the X-ray paucity constraint, can reach values $S_x \gtrsim 10^{-6} - 10^{-7} \text{ ergs cm}^{-2}$ for the brighter bursts, which is above threshold values for typical detectors, if the source is in the field of view.

The optical/UV fluences, again for sources satisfying the canonical X-ray paucity ratio, are predicted to be in the range $S_u \gtrsim 10^{-10} \text{ ergs cm}^{-2}$, and in some cases (e.g. the frozen-in cosmological model) as high as $S_u \gtrsim 3 \times 10^{-8} \text{ ergs cm}^{-2}$ for $D_{28} = 1$, when $S_{\gamma} \sim 3 \times 10^{-6} \text{ ergs cm}^{-2}$. The nearer (brighter) bursts of $S_{\gamma} \sim 10^{-4} \text{ ergs cm}^{-2}$ therefore could have $S_u \sim 3 \times 10^{-6} \text{ ergs cm}^{-2}$, well above HETE’s sensitivity. Other models, e.g. the piston model satisfying both γ -ray observability and X-ray paucity, would predict significantly less UV fluence, e.g. for $S_{\gamma} \sim 10^{-4} \text{ ergs cm}^{-2}$ it predicts $S_u \sim 3 \times 10^{-8} \text{ ergs cm}^{-2}$. The HETE O/UV band limiting sensitivity can also be expressed in U-band magnitudes as $m_{u,m} \sim -2.5 \log_{10}(S_{u,m} \nu_u^{-1} t_L^{-1} / 1.9 \times 10^{-20} \text{ ergs cm}^{-2} \text{ s}^{-1} \text{ Hz}) \sim 11$. for a burst of $S_u/t_L \sim 10^{-9} \text{ ergs cm}^{-2} \text{ s}^{-1}$. The U-magnitude for an arbitrary burst is $m_u = 11. - 2.5 \log_{10}(S_u/10^{-9} \text{ ergs cm}^{-2}) + 2.5 \log_{10} t_L$, where t_L is the observed burst duration in seconds.

The X-ray and UV fluences discussed above are appropriate for the case when a restriction of the type $S_x/S_{\gamma} \lesssim 0.03$ is assumed valid, which requires in general a break at some energy between the γ -ray and X-ray energies. From the Band, *et al.* (1993) analysis, it appears that many of the bursts observed with the spectroscopy detector have breaks at energies ranging from 400 to 100 KeV, and some above that. However, a number of GRB do not show a break within the detector energy range (down to $\sim 50 \text{ keV}$). This implies

that there could be some bursts which have a higher X-ray fluence than that mentioned above, e.g., possibly as much as $S_x/S_\gamma \sim 0.1-1$. If the spectral breaks in some bursts occur in the UV, the O/UV fluence could then be much larger than for those bursts satisfying an X-ray paucity restriction.

We note that the self-absorption cut-off would, in all our models, suppress radio-band emission during the burst, especially in “cosmological” models. There is, however, the possibility of a faint radio “afterglow”, delayed by a few days in the cosmological case, by which time the surface area of the fireball has become much larger (cf. Paczynski and Rhodes 1993). The delay would be shorter for “galactic” models, however, and radio flashes that might be observed could then more plausibly be attributed to coherent pulsar-type emission arising from violent magnetospheric effects around a neutron star.

The fluences at all energies depend, of course, on the assumed electron power law index and the slopes above and below the break s_a , s_b . The extrapolation of our results for slope values other than those used here is straightforward, since the break energies and the fluence at these break points do not change. For the fiducial power per decade slope above the break assumed here, the GeV fluences are usually comparable to the MeV fluence (when the MeV band is near or below the main break). The predicted GeV (or higher energy) fluences could also depend on a high energy cutoff of the electrons. (Above photon energies $\gtrsim 1$ TeV photon-photon opacity effects are likely to reduce the fluences to values below those shown in the figures). The EGRET fluence sensitivity above 1 GeV (Gehrels, *et al.*, 1991) is of the order $S_{\text{GeV}} \gtrsim 10^{-5}$ ergs cm^{-2} (this is a rough extrapolation from the steady source sensitivity for a 5×10^5 s integration; for a burst, the background would need to be evaluated more carefully). The instrument has a ~ 0.6 sr field of view as compared to 4π for BATSE. If the power slope is indeed 0, some of the brighter (MeV) bursts should be detectable by EGRET, and indeed they have been (e.g. Schneid, *et al.*, 1993, Kwok, *et al.*, 1993).

Acknowledgements: This research has been partially supported through NASA NAGW-1522, NAG5-2362 and the Royal Society.

References

- Band, D., *et al.*, 1993, Ap.J., 413, 281
 Begelman, M.C., Mészáros, P. and Rees, M.J., 1993, M.N.R.A.S., 265, L13
 Cavallo, G. and Rees, M.J., 1978, M.N.R.A.S., 183, 359
 Fishman, G., 1993, in *Compton GRO Observatory*, AIP Conf.Proc. 280, eds. M. Friedlander, N. Gehrels and D. Macomb (A.I.P., New York), p. 669
 Gehrels, N., Kniffen, D.A. and Ormes, J.F., 1991, in *Proc. 22nd Int. Conf. on Cosmic Rays*, L. Drury, ed. (University College, Dublin), p...
 Goodman, J., 1986, Ap.J.(Lett.), 1986, 308, L47

- Hartmann, D., *et al.*, 1993, to appear in *High Energy Astrophysics*, J. Matthews, ed. (World Scientific).
- Hudec, R., *et al.*, 1992, in *Gamma-ray Bursts*, A.I.P. Conf.Proc. 265, W. Paciesas and Fishman, G., eds. (A.I.P., New York), p. 323
- Hoshino, M., Arons, J., Gallant, Y. and Langdon, B., 1992, *Ap.J.*, 390, 454
- Katz, J.I., 1993, *Ap.J.*, in press
- Kouveliotou, C., *et al.*, 1993, *Ap.J.(Letters)*, 413, L101
- Kwok, P.W., *et al.*, 1993, in *Compton GRO Observatory*, AIP Conf.Proc. 280, eds. M. Friedlander, N. Gehrels and D. Macomb (A.I.P., New York), p.855
- Laros, J.G., *et al.*, 1984, *Ap.J.* 286, 681
- Meegan, L.A., Fishman, G.J., Wilson, R.B., Paciesas, W.S., Brock, M.N. Horack, J.M., Pendleton, G.N. and Kouveliotou, C., 1992, *Nature*, 335, 143.
- Mészáros, P. and Rees, M.J., 1992a, *Ap.J.*, 397, 570.
- Mészáros, P. and Rees, M.J., 1992b, *M.N.R.A.S.*, 257, 29P.
- Mészáros, P. and Rees, M.J., 1993, *Ap.J.*, 405, 278
- Mészáros, P., Laguna, P. and Rees, M.J., 1993, *Ap.J.*, 215, 181.
- Moskalenko, E.I., *et al.*, 1992, in *Gamma-ray Bursts*, C. Ho, R. Epstein and E. Fenimore, eds. (Cambridge U.P.), p.127
- Murakami, T., *et al.*, 1992, in *Gamma-ray Bursts*, C. Ho, R. Epstein and E. Fenimore, eds. (Cambridge U.P.), p.239
- Narayan, R., Paczynski, B. and Piran, T., 1992, *Ap.J.(Letters)*, 395, L83
- Paczynski, B., 1986, *Ap.J.(Lett.)*, 308, L43
- Paczynski, B., 1990, *Ap.J.*, 363, 218.
- Paczynski, B., 1992, in *Gamma-ray Bursts*, eds. Paciesas, W. and Fishman, G. (A.I.P. Conf.Proc. 265, New York), p. 144
- Paczynski, B. and Rhoades, J., 1993, *Ap.J.(Letters)*, submitted
- Piran, T., Shemi, A. and Narayan, R., 1993, *M.N.R.A.S.*, 263, 861.
- Rees, M.J., 1967, *M.N.R.A.S.*, 137, 429
- Rees, M.J. and Mészáros, P., 1992, *M.N.R.A.S.*, 258, 41P.
- Ricker, G., *et al.*, 1992, in *Gamma-ray Bursts*, C. Ho, R. Epstein and E. Fenimore, eds. (Cambridge U.P.), p. 288
- Ryu, D. and Vishniac, E., 1991, *Ap.J.*, 368, 411.
- Schaefer, B., *et al.*, 1992, *Ap.J.(Lett.)*, 393, L51
- Schneid, E.J., *et al.*, 1993, in *Compton GRO Observatory*, AIP Conf.Proc. 280, eds. M. Friedlander, N. Gehrels and D. Macomb (A.I.P., New York), p.850

Shemi, A. and Piran, T., 1990, Ap.J.(Lett.), 365, L55

Usov, V.V., 1992, Nature, 357, 472

Woosley, S., 1993, Ap.J., 405, 273

Figure Captions

Fig. 1: Cosmological model spectra for a luminosity distance $D_L = 10^{28}$ cm, $E_o = 10^{51}$ ergs, $\theta = 10^{-1}$ and $\eta = 10^3$. The first three are the cosmological frozen-in, turbulent and piston models for an external density $n_0 = 1$ and duration $t_L = 5$ s (top left, top right, bottom left). Identifying models by a label (type-distance, $\log E_o$, $\log \theta$, $\log n_0$, $\log \xi$, $\log \kappa$), these are FC51-1003, TC51-10-63, PC51-10-32. The full lines are the total spectra, and the dashed lines are the spectral sub-components discussed in the text. The fourth spectrum (bottom right, PC51-1n-32) is the cosmological piston for three different densities, $n_0 = 10^{-3}, 1, 10^3$, and durations $t_L = 50., 5., 0.5$ s (left to right). A similar density dependence also holds for the frozen-in and turbulent models.

Fig. 2: Halo model spectra for a distance $D = 50$ Kpc, $\theta = 10^{-1}$. The first three, for $n_0 = 10^{-3}$, are the frozen-in (top left, FH45-1-303) turbulent (top right, TH41-1-303), and piston models (bottom right, PH41-1-303), for two durations, $t_L = 10, 0.5$ s (dashed and full lines). The bottom right figure is the piston halo model PH41-1n03 for densities $n_0 = 10^{-3}, 1, 10^3$ and durations $t_L = 10, 1, 10^{-1}$ s (left to right).

Fig. 3: Galactic disk model spectra for a distance $D = 1$ Kpc, $\theta = 10^{-1}$, showing for $n_0 = 1$ the frozen-in (top left, FD43-1003), turbulent (top right, TD39-1003) and piston (bottom left, PD39-1003) models at two durations $t_L = 5, 0.2$ s (dashed, full lines). In the bottom right figure the piston disk model PD39-1n03 is shown for three external densities $n_0 = 10^3, 1, 10^{-3}$ and durations $t_L = 2, 0.2, 0.02$ s (left to right).

Fig. 4: Frozen-in cosmological model FC51-1003, for an external density $n_0 = 1$ and $D_L = 10^{28}$ cm. The model parameters are FC51-1003, giving (type-distance, $\log E_o$, $\log \theta$, $\log n_0$, $\log \xi$, $\log \kappa$). The lower left flat portion is not part of the spectrum, it represents the HETE threshold at fluence $F \sim 10^{-10}$ ergs cm $^{-2}$. In order of increasing energies, the breaks are due to synchrotron and IC in the reverse shock, and reverse synchrotron photons IC-scattered in the blast wave.

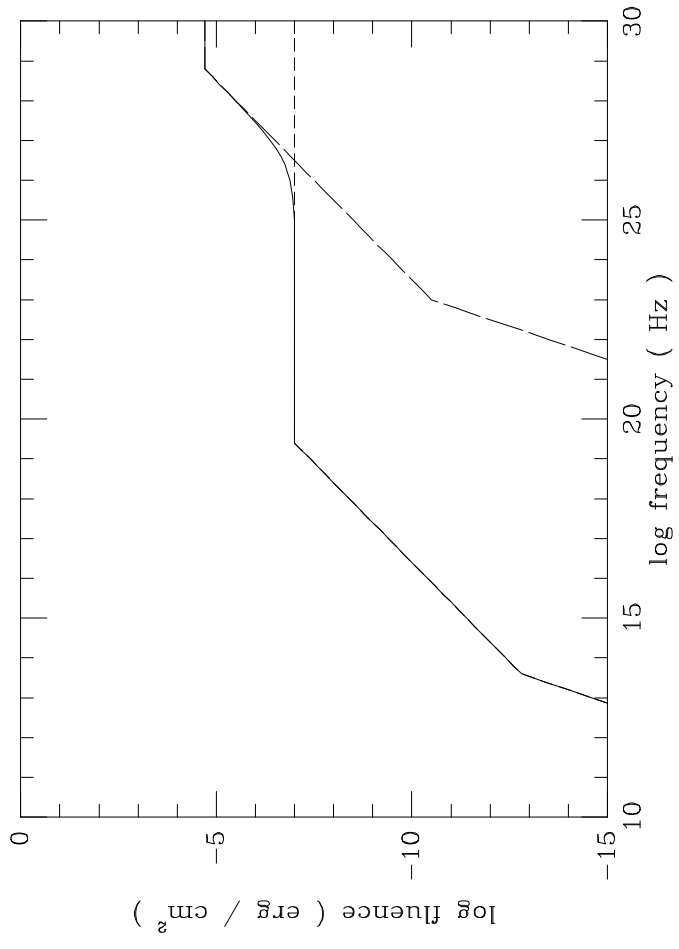
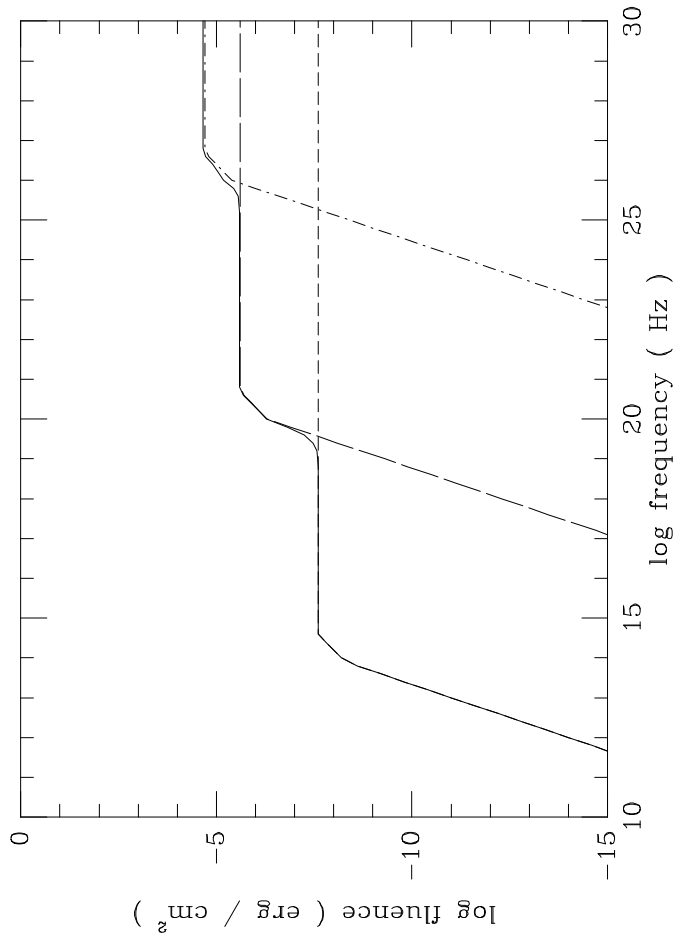
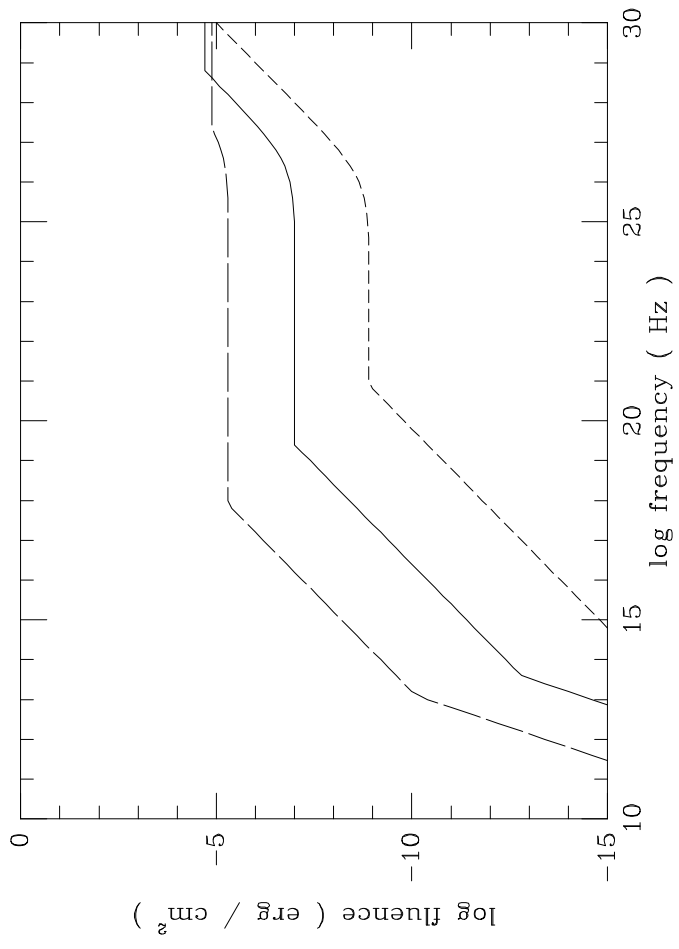
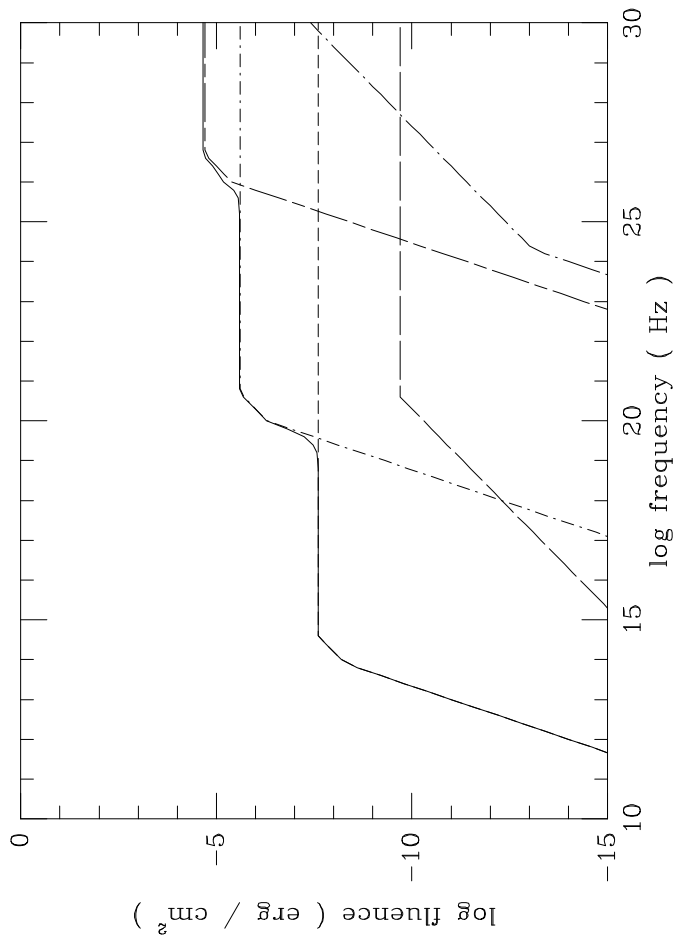
Fig. 5: Turbulent cosmological model TC51-10-63 for $n_0 = 1$, $D_L = 10^{28}$ cm. As before, the detection threshold is at 10^{-10} ergs cm $^{-2}$, in order of increasing energy the breaks are due to synchrotron and IC in the reverse shock, reverse synchrotron photons IC-scattered on the blast wave, and blast wave synchrotron photons IC-scattered in the blast (the blast synchrotron component is submerged by the others).

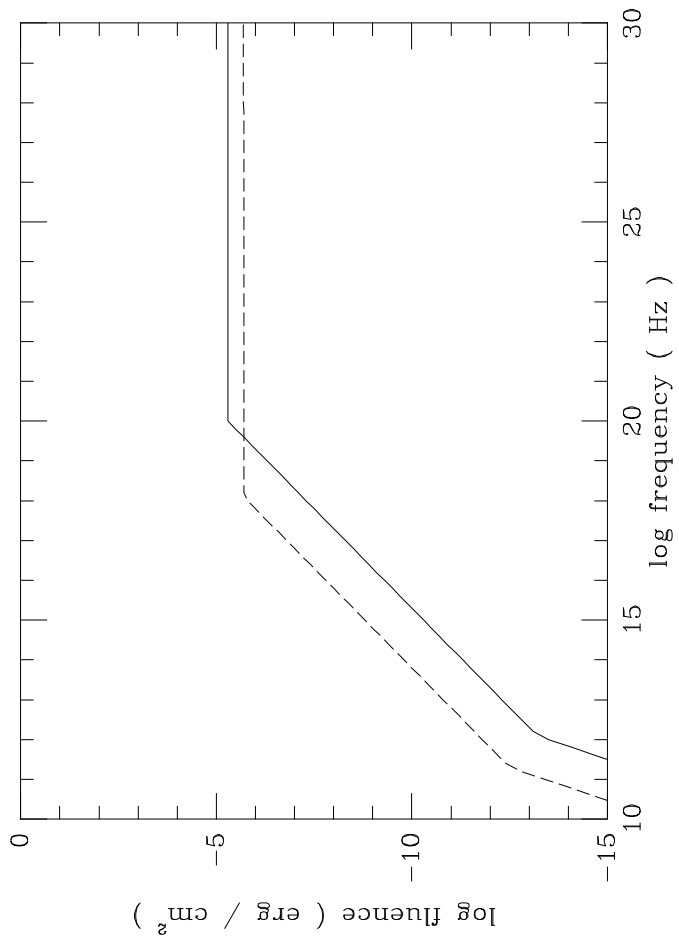
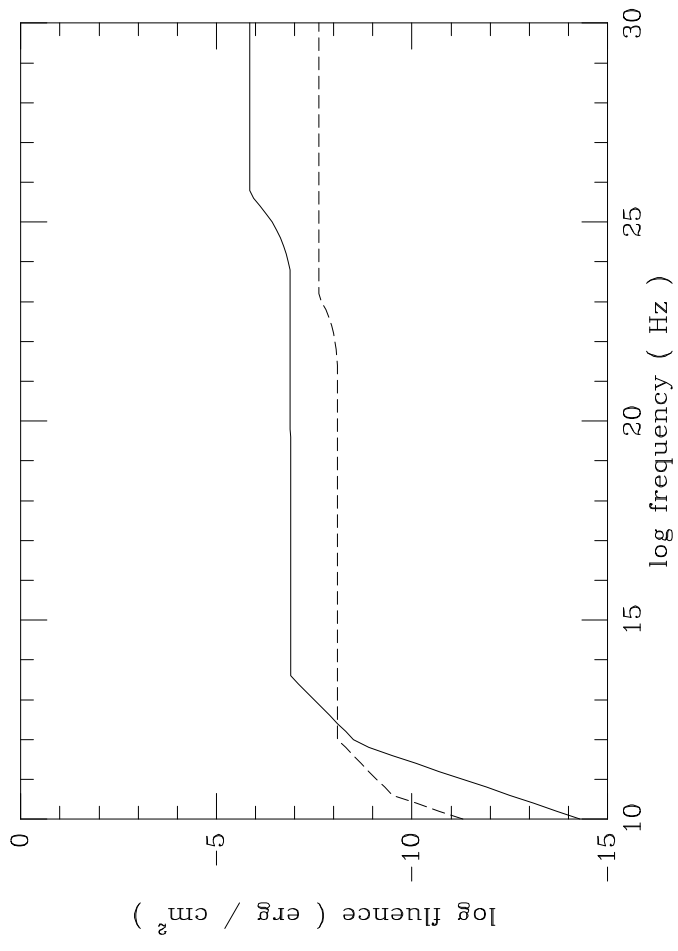
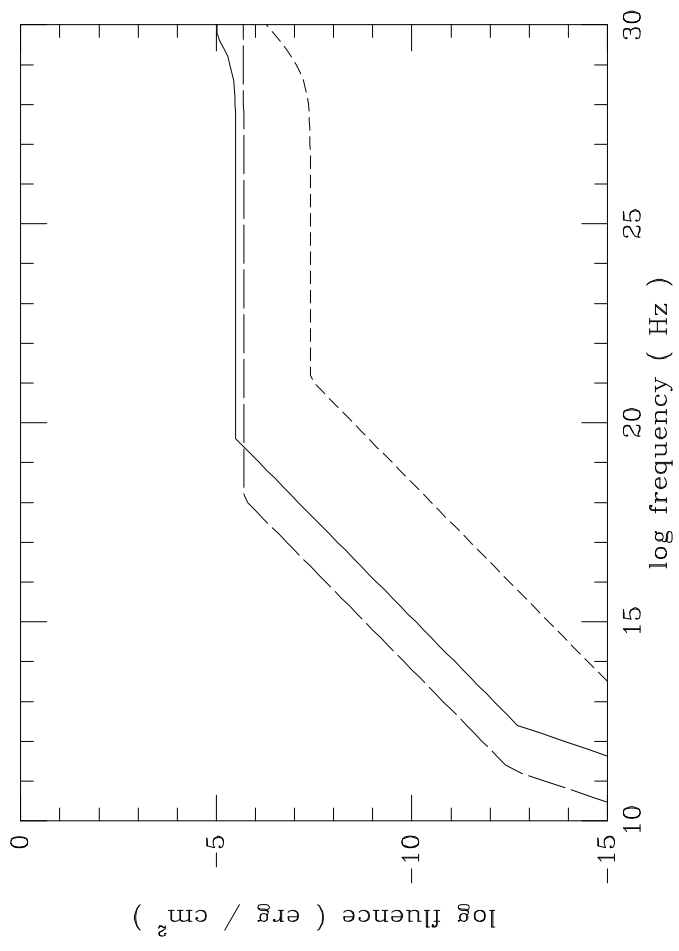
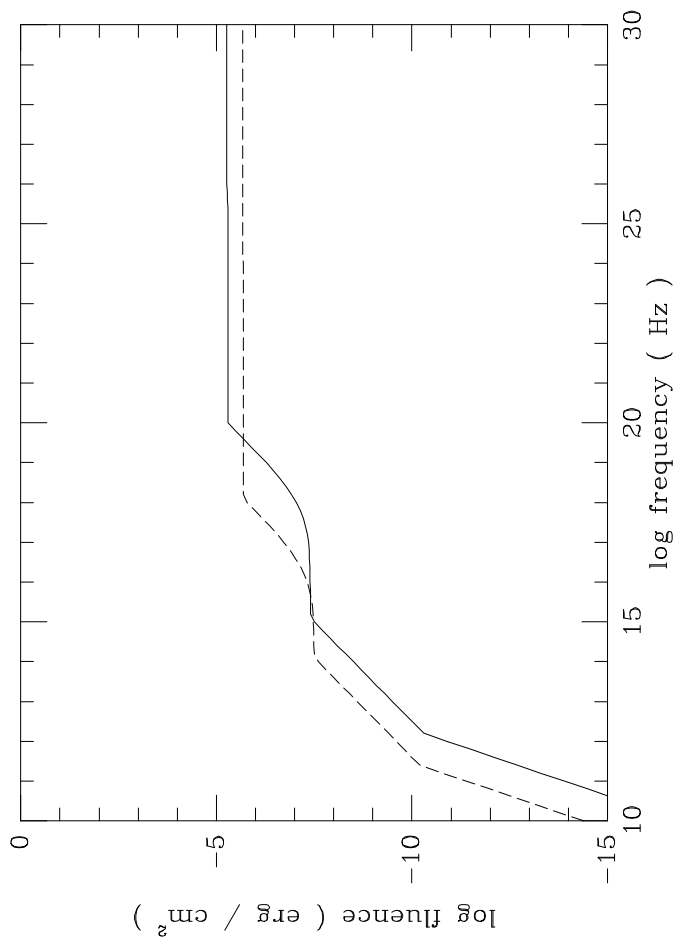
Fig. 6: Turbulent halo model TH41-1-303 for an external density $n_0 = 10^{-3}$ and $D = 50$ Kpc. Detection threshold is 10^{-10} ergs cm^{-2} . The main breaks seen are the reverse synchrotron, blast synchrotron and combined IC (barely seen at low durations), with increasing energies.

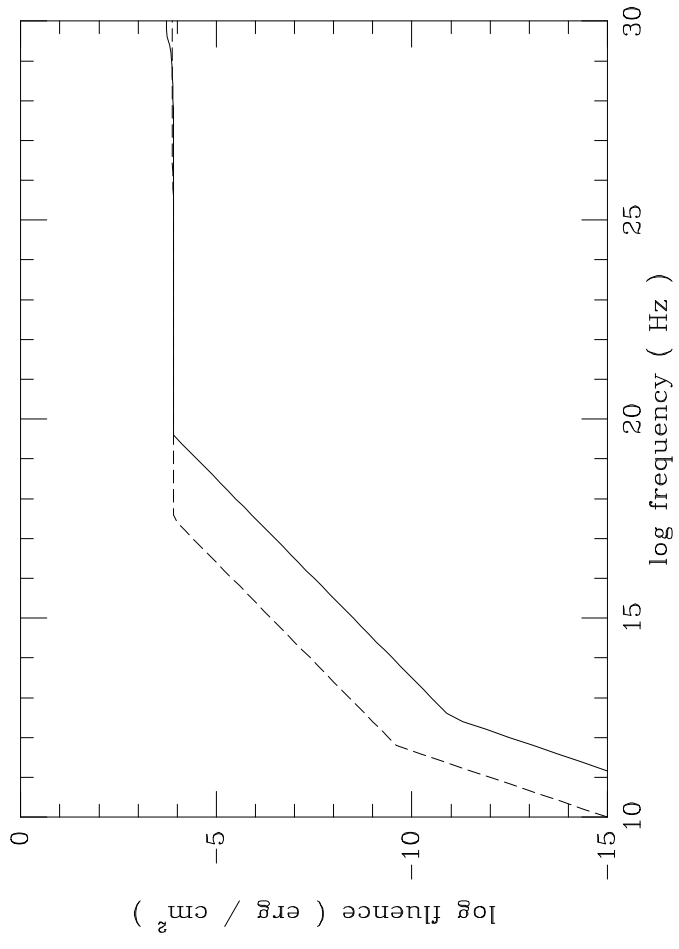
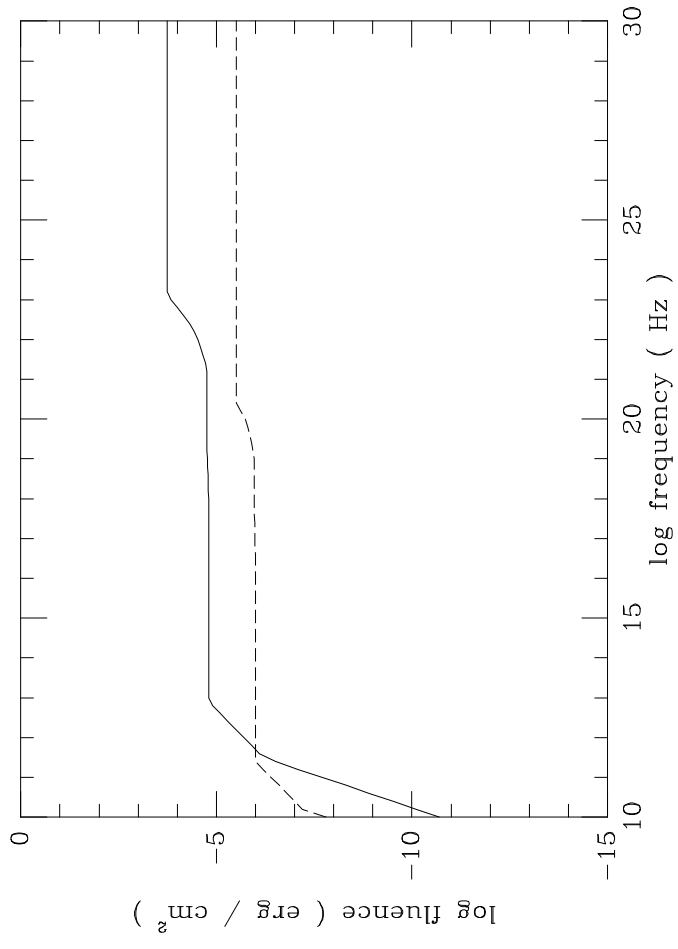
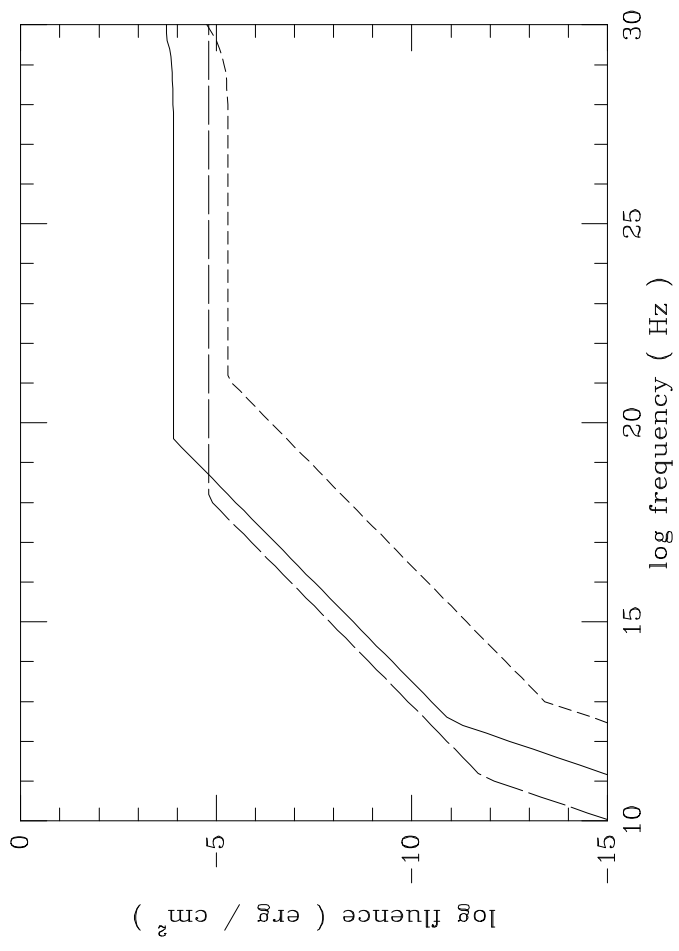
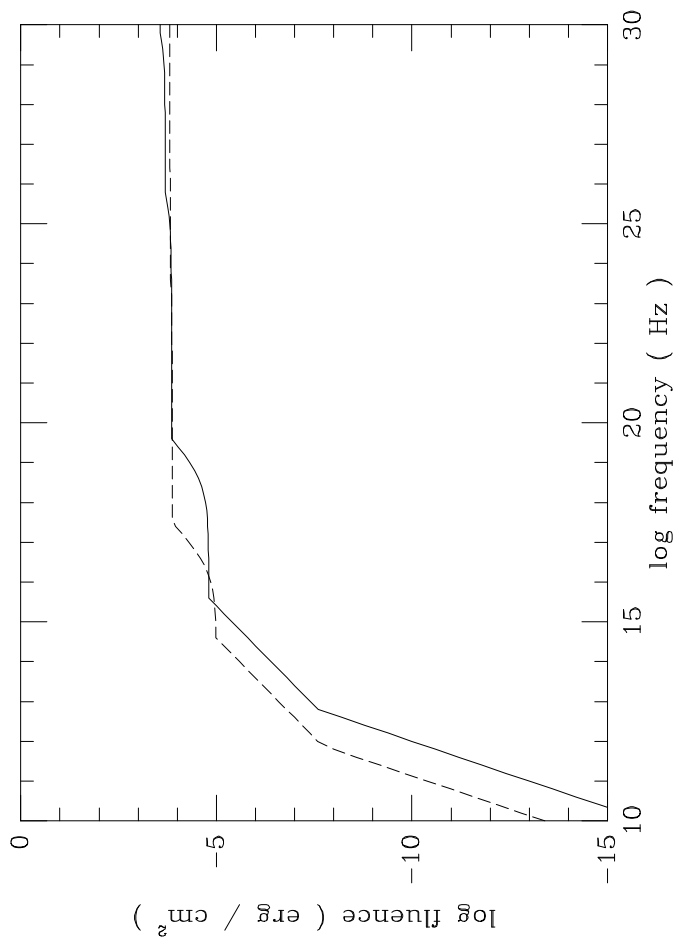
Fig. 7: Piston Cosmological model PH51-10-32 for an external density $n_0 = 1$, and detection threshold at 10^{-10} ergs cm^{-2} . The two breaks are due to synchrotron and IC photons from the blast.

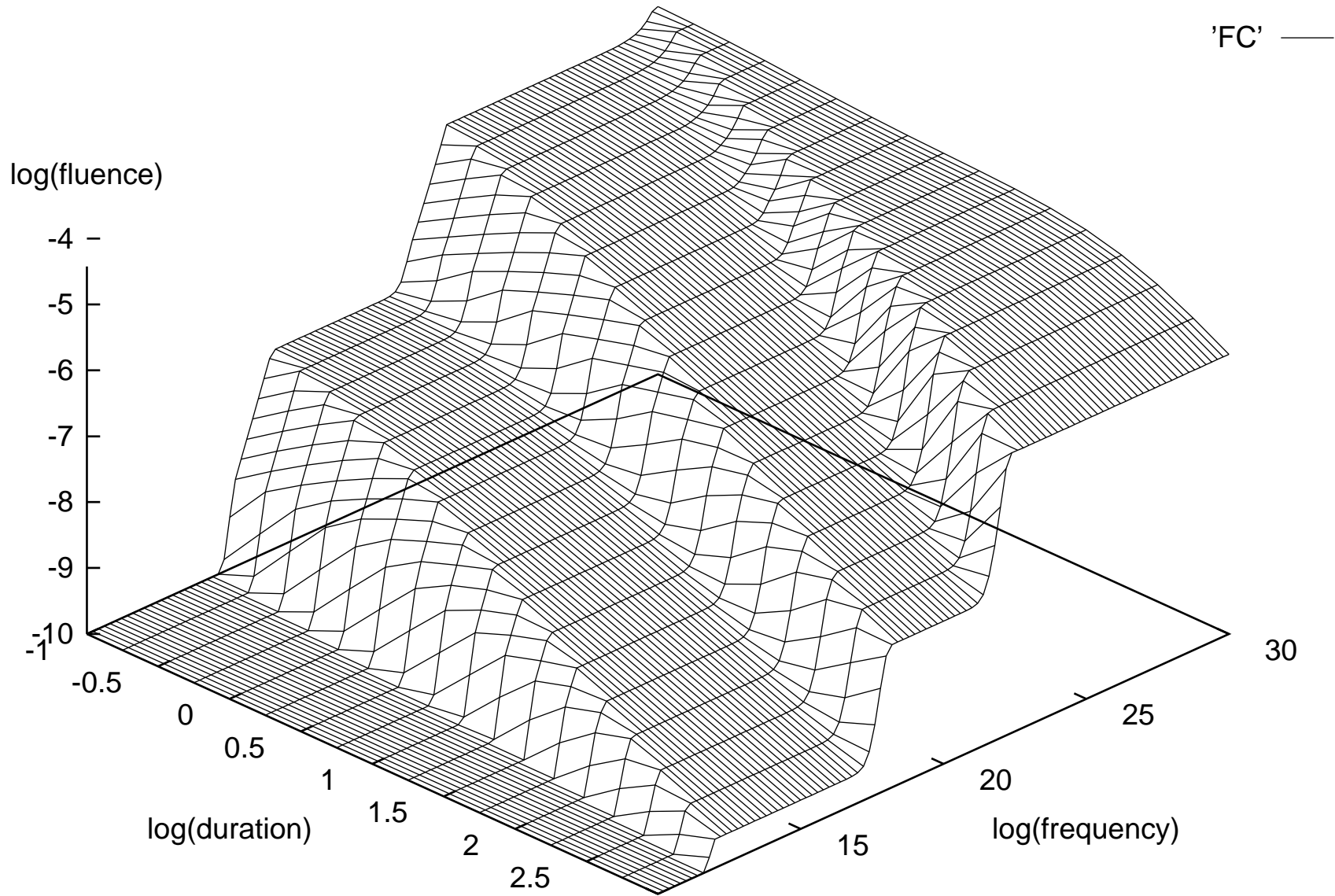
Fig. 8: Piston (galactic) disk model PD39-1003, for an external density $n_0 = 1$, distance $D = 1$ Kpc and detection threshold 10^{-10} ergs cm^{-2} . The main break is due to the blast wave synchrotron photons, while the blast wave IC is at very high energies, and relatively weaker.

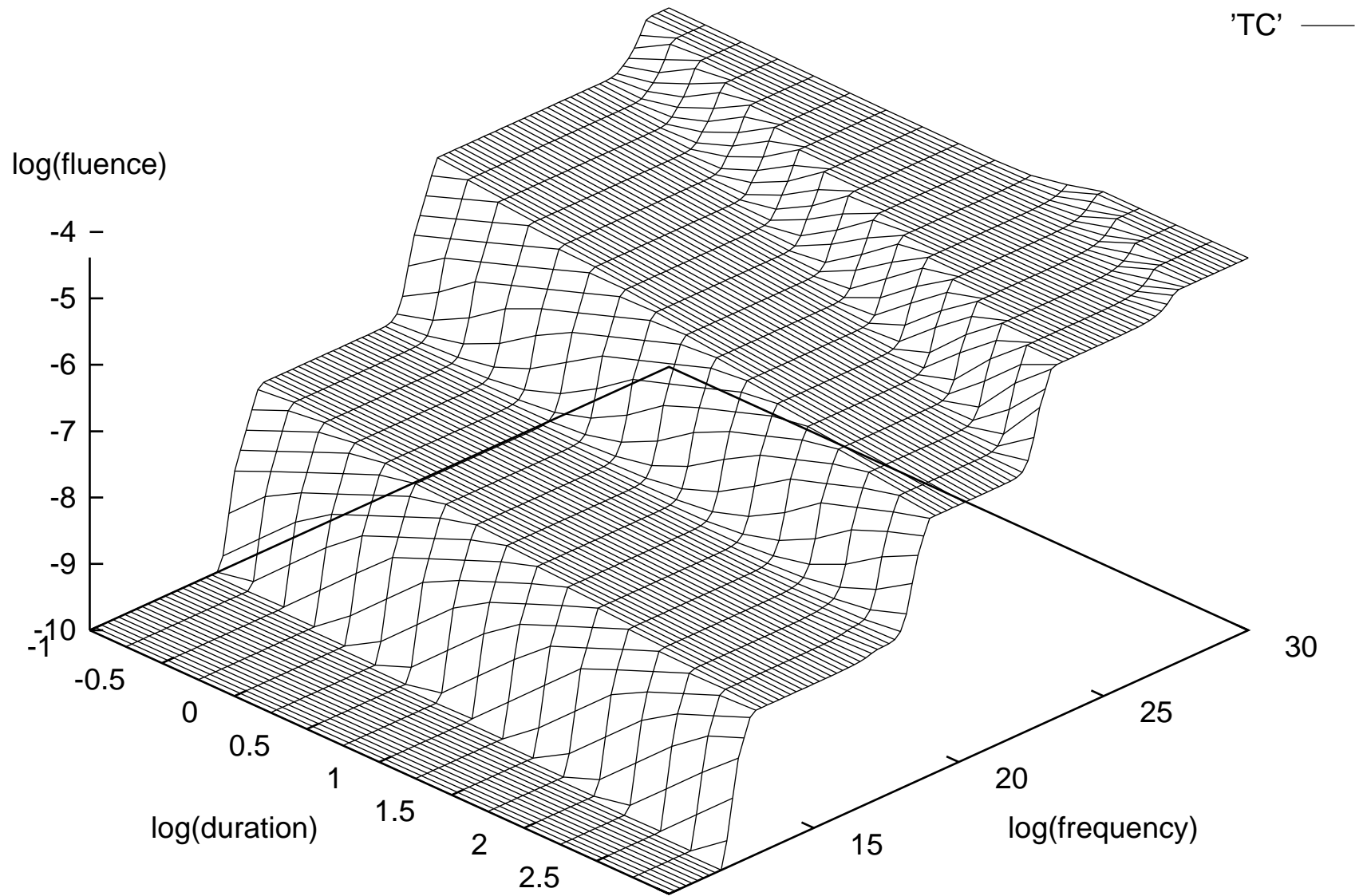
Fig. 9: The γ -ray band (0.5 MeV) fluence contours and the γ -ray to X-ray band fluence ratios (0.5 MeV/1 KeV), in the duration-external density parameter space, for the three types of model F, T, P (columns) at the three distance scales C, H, D (rows). The γ fluence has three contour levels, $S_\gamma = 10^{-8}, 10^{-6}, 10^{-4}$ ergs cm^{-2} (dotted, short-dashed and long-dashed lines, unlabeled); the γ/X ratio has three contour levels, $\log S_\gamma / \log S_x = 1., 1.5, 2.$ (dot-dash, dot- long dash, and dotted, with label r). In the halo and galactic disk cases, models below and to the left of the solid diagonal line have $\eta > \Gamma_{max} = 3.3 \times 10^2 E_{42}^{1/3} r_6^{-2/3}$ (see text), i.e., they don't satisfy the impulsive approximation; in this region, the duration t_L is not given by eq.(2.1.4) as plotted, but must be specified as an additional free parameter.

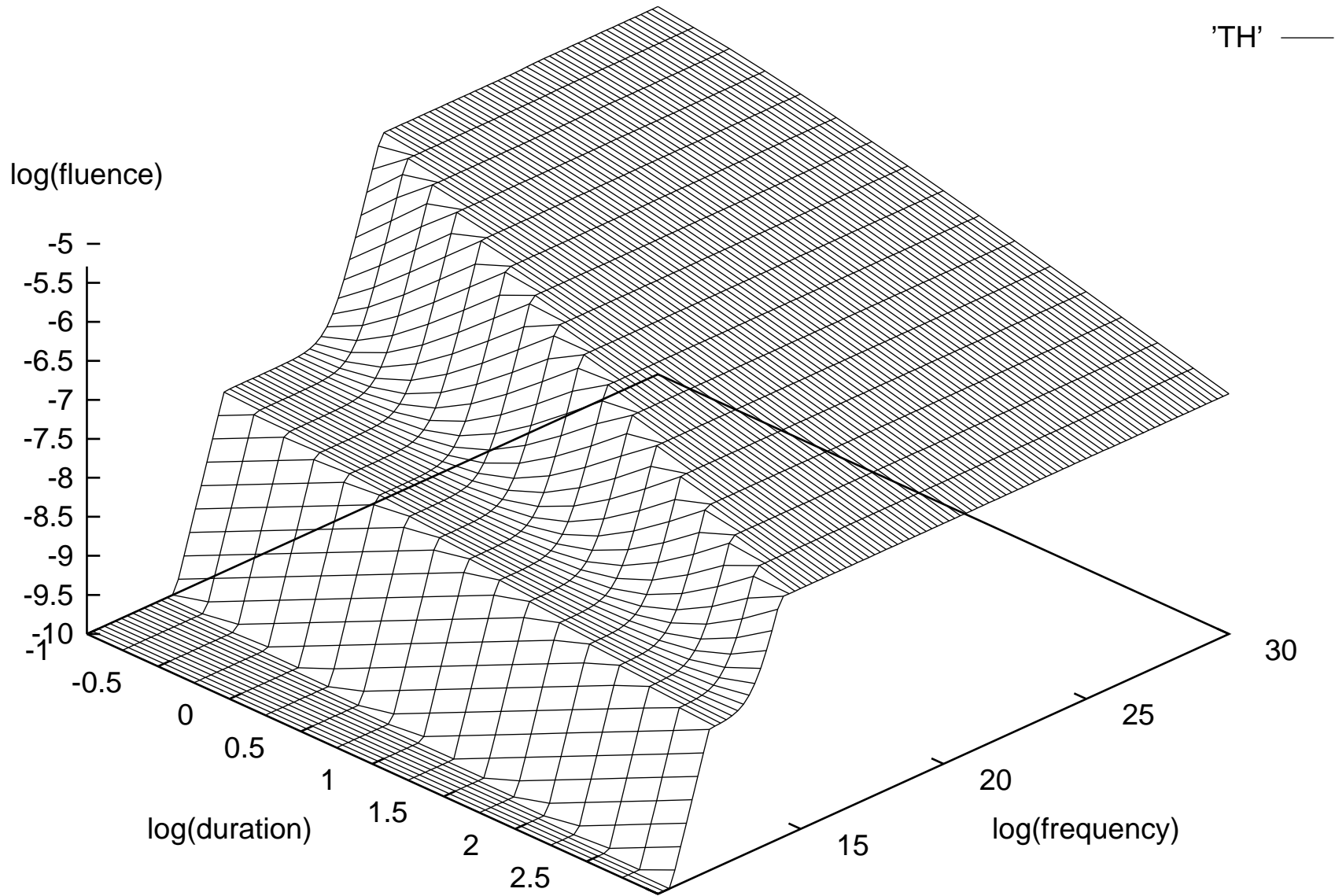












PC

